Volume-shrinking kinetics of transient gels as a consequence of dynamic interplay between phase separation and mechanical relaxation

Takehito Koyama and Hajime Tanaka[*]

Institute of Industrial Science, University of Tokyo, 4-6-1 Komaba, Meguro-ku, Tokyo 153-8505, Japan

Gels are very important states of matter in our life and can be classified into three types: chemical, stable physical, and transient gels. The first two are formed by the percolation of chemical and physical bonds, respectively, and practically have an infinite lifetime, meaning that they have nonzero static shear moduli and behave as soft solids. On the other hand, the last one is formed only transiently during demixing of a dynamically asymmetric mixture composed of large (slow) and small (fast) components. It emerges as a transient percolated network of the large components, and accordingly it has a finite lifetime (or, it eventually behaves as a liquid). Although the states of chemical and physical gels are reasonably well understood, the physical understanding of transient gelation has remained very poor; for example, a mechanical boundary condition originating from *transient elasticity* has not been considered before. The fundamental difficulty originates from the fact that transient gelation is a dynamically evolving nonequilibrium process as a consequence of complex dynamical interplay between phase separation and mechanical relaxation (or rheology), but there is no reliable theory for the rheology of a nonequilibrium system. To overcome this difficulty and elucidate the physical essence of transient gelation, we combine experimental and theoretical approaches to study the volume-shrinking kinetics of a transient gel and compare it with that of a permanent chemical gel undergoing a volume phase transition. We reveal that the volume-shrinking behavior of a transient gel is fundamentally different from that of a chemical gel. A permanent gel has static elasticity coming from its permanent network topology. In contrast, a transient gel is formed by hierarchical structure formation (polymers → globules → percolated network) and is stabilized only by weak van der Waals bonding between globules, and thus it does not have static elasticity and its elasticity decays with time: viscoelastic relaxation. This relaxational feature leads to the switching of the relevant order parameter during phase separation in the order of scalar (composition), tensors (volume and shear deformations), and scalar (composition). Depending on the relation of the deformation rate generated by phase separation itself to the bulk and shear mechanical relaxation rates, a transient network behaves liquid-like, viscoelastic, and elastic; leading to liquid-like, ductile, and brittle fracture of the network during shrinking, respectively. We also find that the emergence of elasticity during transient gelation is the reverse of its disappearance and there is a one-to-one correspondence between them, strongly indicating the key role of viscoelastic relaxation in transient gelation. We argue that these basic features should be generic to any demixing-induced transient gels of soft matter, including polymer solutions, colloidal suspensions, emulsions, and biological solutions such as protein solutions. Our finding not only sheds new light on the physical nature of this intrinsically nonequilibrium transient state of matter but also provides the physical basis for demixing of soft- and bio-matter.

I. INTRODUCTION

A transient gel is formed when a dynamically asymmetric mixture composed of large (slow) and small (fast) components undergoes phase separation [1,2]. Such dynamically asymmetric mixtures include polymer solutions, colloidal suspensions, emulsions, and biological solutions such as protein solutions. A transient gel is nothing but a transient percolated network of the large components of such a mixture. In this type of phase separation, even the slow-component-rich minority phase can transiently form a percolated network structure, contrary to the common rule of normal phase separation [3] that the minority phase always forms isolated droplets to minimize the interfacial energy.

This unconventional phase separation caused by the dynamical coupling between composition and stress fields is called "viscoelastic phase separation" (VPS) [1,2]. This type of phase separation is widely observed in various fields such as materials science [4,5], food science [6,7], bioscience [8,9], medical science [10], and geoscience [11,12]. Very recently, liquid-liquid phase separation in biological cells has attracted considerable attention after the discovery of non-membrane-bounded domain structures termed membrane-less organelles in cells [13–20]. Because these domains are formed by concentrated macromolecular and protein solutions, viscoelastic effects may play a crucial role during phase separation. For example, Iborra [21] argued that nuclear compartmentalization can be explained by viscoelastic phase separation of the dynamically different nuclear components, in combination with macromolecular crowding and the properties of colloidal particles.

———————
[*]tanaka@iis.u-tokyo.ac.jp

Thus, transient gelation is an extremely important phenomenon that may take place in any mixture with strong dynamical asymmetry between the components. Despite its significance, however, their macroscopic behavior—their formation, the evolution of elasticity, and final relaxation back to a fluid state—has not been explored yet, and thus the physical mechanism behind this complex dynamical process has remained elusive. The fundamental difficulties arise from the fact that, unlike a chemical gel, (i) a transient gel only appears during phase demixing and thus is essentially heterogeneous, and (ii) it does not possess static elasticity and its elasticity is intrinsically transient, since it is a consequence of viscoelastic effects; that is, the dynamical crossover between the deformation rate induced by phase separation and the internal rheological relaxation rate. For example, the internal structure of a transient gel and thus its viscoelastic properties are almost completely unknown, unlike the case of a chemical gel.

The network of a transient gel is formed only during phase separation by transient bonding, different from that of a permanent chemical gel formed by intermonomer covalent bonding. Thus, it is natural to think that the origin of the elasticity of a transient gel is basically dynamical and that its mechanical behavior depends on the relation between the characteristic time of deformation induced by phase separation itself, τ_d, and the bulk and shear relaxation times of the network, τ_B and τ_S, respectively [1,2]. Just like in ordinary viscoelastic matter [22,23], a system can be regarded as elastic for $\tau_d \ll \tau_B, \tau_S$, viscoelastic for $\tau_d \sim \tau_B, \tau_S$, and fluid for $\tau_d \gg \tau_B, \tau_S$. Here we note that the term "bulk" deformation represents the deformation of the volume occupied by a transient gel network, which must be accompanied by the transport of the solvent: The volume increase and decrease of a transient gel is realized only through absorbing or expelling the solvent, respectively. To show the relevance of this idea, we need to compare experiments with theories in a quantitative manner. However, such studies have not been performed so far, because of difficulties associated with the intrinsically nonequilibrium nature of a transient gel. We stress that it is extremely difficult to develop a microscopic rheological theory for an unstable state of matter undergoing spinodal decomposition.

In this paper, we aim to reveal the physical nature of a transient gel and its dynamical evolution during phase separation. To do so, we experimentally study the volume-shrinking kinetics of freely shrinking cylindrical transient gels formed in polymer solutions undergoing phase separation. We successfully studied the volume-shrinking kinetics quantitatively for the first time. By comparing these results with a theory as well as the known results of volume shrinking in permanent chemical gels [24–32], we elucidate how elasticity emerges during the formation of a transient gel and how the transient elasticity decays in the viscoelastic relaxation process. We show that the sequential fluid-to-solid and solid-to-fluid transition during the phase demixing process of a polymer solution can be fully explained by the concept of spontaneous viscoelastic relaxation in phase separation; more specifically, as a consequence of dynamical crossover of the domain deformation rate, τ_d^{-1}, with bulk and shear mechanical relaxation rates, τ_B^{-1} and τ_S^{-1}. We also reveal that

hierarchical structure formation upon transient gelation (polymers → globules → network formation) not only plays a pivotal role in the presence of independent dynamical crossover behavior for bulk and shear modes, but is also responsible for unique viscoelastic properties of a transient gel.

II. EXPERIMENT

The systems studied were mixtures of monodisperse polystyrene (PS) and diethyl malonate (DEM). Note that PS, being an atactic polymer, neither crystallizes nor forms any stable bonds between chains. We mainly used two PSs with the weight-average molecular weights (M_w) of 7.04×10^5 (PS1) and 3.84×10^6 (PS2). The molecular weight distributions M_w/M_n (M_n is the number-average molecular weight) were 1.05 (PS1) and 1.04 (PS2).

For observation of a volume-shrinking process of a transient gel in a polymer solution, we insert the sample into a cylindrical tube and quench it into an unstable region of the solution. See the Appendix for the details of our experimental and analysis methods.

A. Phase diagram

The PS-DEM mixtures have upper-critical-solution-temperature (UCST) type phase diagrams [1,2,22,33], which are shown as a function of the temperature T and the initial PS composition ϕ_0 in Fig. 1(a) for PS1-DEM and in Fig. 1(b) for PS2-DEM. The critical composition ϕ_c and temperature T_c of the mixtures were determined to be 4.1 wt% PS1 and 22.3 °C for PS1-DEM and 2.1 wt% PS2 and 27.2 °C for PS2-DEM [34]. The dependence of the phase-separation behavior near ϕ_c on the degree N of polymerization is shown in Fig. 1(c). The theta temperature Θ [note that $\Theta = T_c(N)$ in the limit of $N \to \infty$] [22,33] of the PS-DEM mixtures is $\sim$32.2 °C [34].

B. Three types of viscoelastic phase separation

When a polymer solution is quenched slightly below the binodal line, where dynamical asymmetry is weak enough, ordinary phase separation takes place. When a solution with $\phi_0 \gtrsim \phi_c$ is quenched below the spinodal line, the system becomes unstable and spinodal decomposition takes place. Here we show typical pattern evolution processes during spinodal decomposition observed in quasi-two-dimensional (2D) thin films of mixtures of PS and DEM in Figs. 2(a)–2(c). In these experiments, the edge of a sample is fixed. Because of this fixed boundary condition, the macroscopic volume shrinking of the entire sample does not take place; instead, the volume shrinking of the polymer-rich phase proceeds by creating solvent holes in the PS-rich phase. In our phase-contrast microscopy observation, the dark domains are the PS-rich phase, whereas the bright domains are the DEM-rich phase. We also show in the phase diagrams in which region each type of VPS is observed (see Fig. 1). As shown in Fig. 1, we can classify spinodal decomposition into the following three types:

(i) Weakly viscoelastic phase separation (wVPS): For wVPS [see Fig. 2(a)], the solvent-rich phase forms droplets rather than a bicontinuous structure, even though the volume
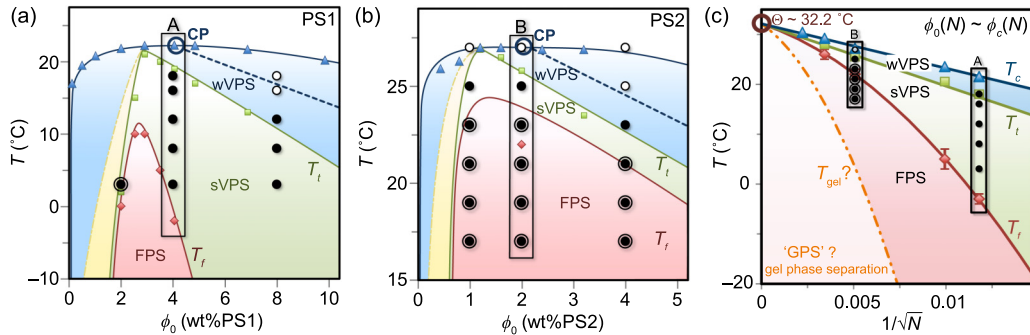
FIG. 1. Various types of phase separation behavior observed in PS-DEM solutions. Panels (a) and (b) show the state diagrams for PS1-DEM and PS2-DEM mixtures, respectively. The regions where the three types of phase separation, wVPS, sVPS, and FPS, are observed [see Figs. 2(a)–2(c)] are also indicated in the phase diagrams with the same labels. Triangles show the binodal line [34], squares show T_t below which transient gelation takes place (Refs. [34,35]), and diamonds show T_f below which FPS takes place (Ref. [35] and Appendix 2). The circles labeled "CP" indicate the critical points (see Appendix 2). The dashed straight lines are the lines of the symmetric composition [1,2]. The three types of circular symbols correspond to the three types of VPSs [see Figs. 2(a)–2(c)] and volume-shrinking behavior [Figs. 3–5]. Open circles show wVPS [Figs. 2(a) and 3], black-filled circles show sVPS [Figs. 2(b) and 4], and black double circles show FPS [Figs. 2(c) and 5]. Rectangular boxes labeled A and B indicate the state points near the critical composition ϕ_c. The dashed-dotted curves at the low ϕ region indicate the boundary between network-forming and droplet-forming phase separation [35], the latter of which is not discussed here. Panel (c) shows the N dependence of T_c, T_t (Ref. [34]), and T_f at the critical compositions. Points in rectangular boxes A and B are common to those in panels (a) and (b), respectively. The dashed-double dotted line indicates the expected onset temperature T_{gel} of gel-type phase separation ("GPS"), which will be discussed later. The regions where wVPS and FPS take place are shaded by light blue and red colors, respectively. The light green region in the right-hand side of panels (a) and (b) indicates a sVPS region, where a percolated network (or transient gel) is directly formed through the growth of concentration fluctuations. The light yellow region in the left-hand side of panels (a) and (b), on the other hand, indicate a sVPS regions, where droplets are formed first and then they form a percolated network (or transient gel) later. The light-orange region in panel (c) indicates the region of gel phase separation.

fraction is not so low. This is a consequence of both viscoelastic and wetting effects (see Appendix 2 on the latter effect). The mechanical stress plays a role only in the initial stage and the domain coarsening in the late stage, primarily driven by interfacial tension as in ordinary phase separation: collisions between droplets and the resulting coalescence lead to the domain coarsening. The domain shape is always rounded in wVPS.

(ii) Strongly viscoelastic phase separation (sVPS): In sVPS [see Fig. 2(b)], the minority phase forms a transient gel state just after the temperature quench, which shrinks its volume by creating solvent holes and expelling the solvent to them (see the leftmost image). Then, the volume of the polymer-rich phase keeps shrinking, leading to the formation of a well-developed network structure of the minority polymer-rich phase, whose shape is determined by the mechanical force balance condition (see the third image). The coarsening of the network structure of the polymer-rich phase takes place via liquid-type or ductile fracture of strands of the network due to the concentration of the self-generated mechanical stress on weak parts of the network [1,2,34,35]. In the final stage, however, the interfacial tension starts to play a major role since the system approaches the final equilibrium state and the mechanical stress decays, reflecting the slowing down of the deformation rate generated by phase separation. Accordingly, the domain shape becomes rounded (see the rightmost image).

(iii) Fracture phase separation (FPS): In FPS [see Fig. 2(c)], brittle fracture of the transient gel is the major coarsening mechanism [35]. A deformation rate created by demixing (or a strong shrinking tendency) due to interpolymer attractions is much faster than the relaxation rate of the

polymer solution, leading to a solid-like brittle fracture: formation of cracks and its growth (see the leftmost image). Reflecting the brittle nature of fracture, solvent holes have a crack-like anisotropic shape unlike the rounded shape in sVPS. The large degree of the volume shrinking is a manifestation of the large magnitude of the self-generated internal mechanical stress. After crack formation, the polymer-rich phase keeps expelling the solvent and shrinks its volume. After a very long time, the effects of viscoelasticity will disappear and thus the interface tension should play a major role finally. But this final relaxation takes place much later than 40 min.

These three types of VPS, wVPS, sVPS, and FPS, correspond to liquid-type, ductile, and brittle fracture of amorphous materials, respectively [35,36]. For all cases, the origin of the mechanical instability is commonly *strong dynamical asymmetry for the change of an order parameter* (composition and density, respectively, for phase separation and material fracture) [1,2,36–38]. The only difference between transient gels and amorphous materials is that, for the former, the deformation is self-generated by demixing whereas for the latter it is applied externally. In the next section, we show what kind of volume-shrinking behavior is observed under *the free boundary condition*, corresponding to these three types of VPS shown in Fig. 2 for *the fixed boundary condition*.

III. RESULTS

A. Methods to characterize volume-shrinking behavior

To characterize the volume-shrinking behavior of a cylindrical transient gel, we study the temporal changes of the following four physical quantities (see Appendixes 3 and 4):
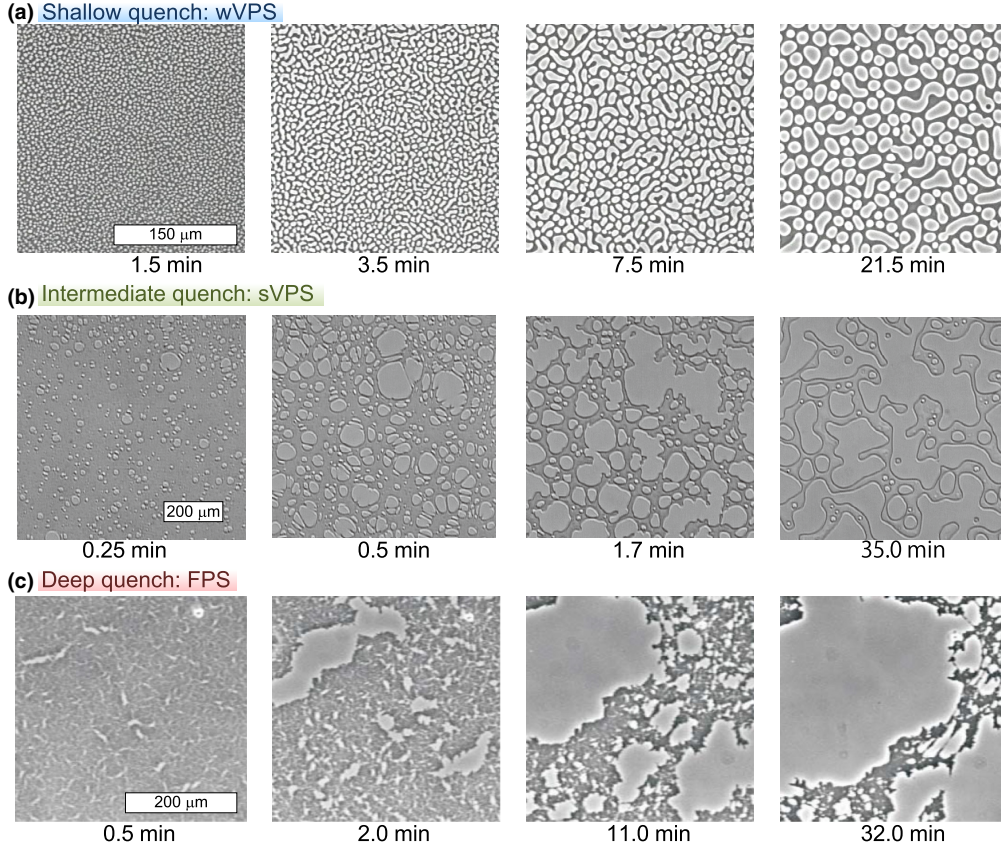
FIG. 2. Typical phase-contrast-microscopy images of the temporal change of phase-separated structures characteristic of (a) wVPS [21.5 °C for 4 wt% PS1; see Fig. 1(a)], (b) sVPS (0 °C for 8.53 wt% PS; $M_w = 1.9 \times 10^5$), and (c) FPS (−2 °C for 4 wt% PS2). The dark domains are the PS-rich phase, whereas the bright domains are the DEM-rich phase (see Appendix 2). In these experiments, the samples were sandwiched between two cover glasses and thus were quasi-two-dimensional, and the boundaries of the samples were clamped by the edges of the cover glasses.

(1) the scaled length $\Delta \ell(t) = [\ell(t) - \ell_f]/(\ell_0 - \ell_f)$, where $\ell(t)$ is the length of a cylindrical gel along its long axis, and its initial and final values are respectively denoted ℓ_0 and ℓ_f; (2) the scaled width (or diameter) $\Delta w(t)$, which is defined in the same manner as $\Delta \ell(t)$; (3) the average transmitted light intensity through a cylindrical tube, $\langle I(t) \rangle$; and (4) the intensity fluctuation amplitude $[\langle \Delta I^2(t) \rangle]^{1/2}$. Both $\Delta \ell(t)$ and $\Delta w(t)$ characterize the change in the outer shape of transient gels (see Appendix 4 a and Figs. 12 and 13), whereas both $\langle I(t) \rangle$ and $[\langle \Delta I^2(t) \rangle]^{1/2}$ characterize the change in the internal structure (see Appendix 4 b and Fig. 14).

From the observation of phase-separation behavior of quasi-2D systems (see Fig. 2), we find that there are three types of deformation behavior, depending upon the initial average composition of the polymer ϕ_0 and the quench depth $\Delta T = T_c - T$, i.e., the temperature distance from the critical temperature T_c. We confirm that these three types of volume-shrinking behavior (shown in Figs. 3–5) have one-to-one correspondence to the three types of pattern evolution of quasi-2D samples shown in Figs. 2(a)–2(c) respectively, i.e., wVPS [open circles in Figs. 1(a) and 1(b)], sVPS (black filled circles), and FPS (double circles). In the following, we qualitatively describe the characteristics of the three types of shrinking behavior of cylindrical transient gels one by one.

B. Case of weakly viscoelastic phase separation

For wVPS [see Fig. 3(a)], the system immediately becomes very turbid and the image becomes very dark after a quench, but quickly becomes brighter when the internal phase-separation structure is visible. This change in the brightness of the image is caused by the crossover between the wavelength of light and that of the internal structure. This can be seen by the temporal change in $\langle I \rangle$ and $(\langle \Delta I^2 \rangle)^{1/2}$ [see Fig. 3(b)]: Both $\langle I \rangle$ and $(\langle \Delta I^2 \rangle)^{1/2}$ steeply decrease almost to zero immediately after quenching, suggesting the steep increase in turbidity upon the initiation of phase separation. We call this process "regime i." This regime i is already finished before the leftmost image of Fig. 3(a). After a short time t_0, these quantities start to gradually increase, whereas $\Delta \ell$ decreases exponentially with time [see the red fitted curve in Fig. 3(b)]. We call this process "regime I." As shown below, viscoelastic stress plays a role only in regime i and has already decayed in regime I. Reflecting this, there is almost no temporal volume change of the PS-rich phase in the late stage of regime I [Fig. 3(c)], which is a typical late-stage demixing behavior of a fluid mixture [3]. The quick decay of the mechanical stress can also be confirmed from the fact that the outer shape of the big polymer-rich domain becomes rounded. Although there is almost no volume change in the
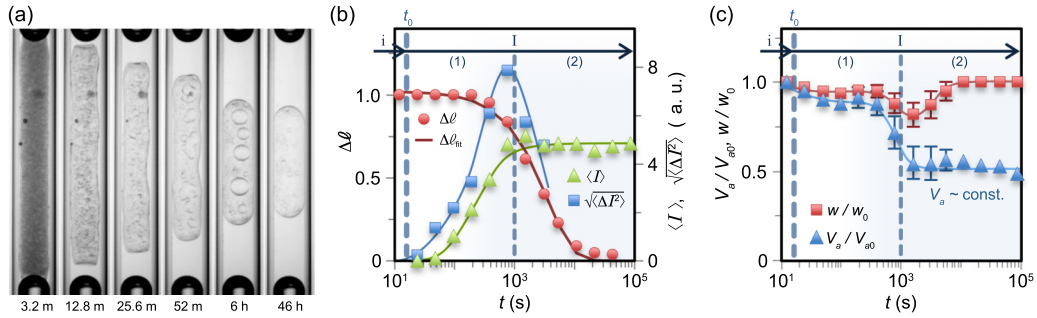
FIG. 3. Volume-shrinking dynamics of a transient gel in wVPS, which is observed at $16\,^\circ$C for 8 wt% PS1 [see Fig. 1(a)]. (a) Back-illuminated images of sample tubes. We can see the PS-rich transient gel of darker contrast in the cylindrical glass tube (inner diameter: 1 mm) (see Video 1 in the Supplemental Material [39]). (b) Volume-shrinking dynamics characterized by the scaled length $\Delta\ell(t)$, the average light intensity $\langle I \rangle$, and the variance of the light intensity fluctuations $(\langle I^2(t) \rangle)^{1/2}$ of the PS-rich transient gel phase. See Appendix 4 b for the definitions of $\langle I \rangle$ and $(\langle I^2(t) \rangle)^{1/2}$. (c) Temporal change of both the width ratio w/w_0 and the apparent volume ratio V_a/V_{a0} calculated as $w^2\ell/(w_0^2\ell_0)$. We use the mean values of V_a/V_{a0} and of w/w_0 between its maximum and minimum represented by the endpoints of the error bars (those smaller than the size of the indicator of the data points are not shown). The errors are due to shape fluctuations of the PS-rich phase shown in panel (a). Regime I is further divided into regime (1) and (2), although this division is not essential (see text). We note that, although divided into these two subregimes, regime I is characterized by the single exponential decrease of $\Delta\ell$ with the characteristic decay time τ^1 (see the fitted curve $\Delta\ell_{\rm fit}$ and Sec. VI B 1). We identify regime i before t_0 and regime I after t_0 (see Appendix 4 a). Solid lines without legends are to guide the eye.

PS-rich phase itself, the volume of the outer shape apparently shows the volume decrease [see Fig. 3(c)]. Reflecting this behavior, we divide regime I further into two regimes [see Figs. 3(b) and 3(c)]: In regime (1) there is an apparent volume change, but this is due to escape of solvent-rich droplets from the PS-rich domain (not the volume shrinking of the PS-rich phase itself). In regime (2), on the other hand, the volume is almost constant since the DEM-rich phase is confined as large droplets inside the large PS-rich domain [see Fig. 3(a)]: the slight decrease of V_a/V_{a0} after 10^4 s is again due to the escape of a few large droplets from the PS-rich domain (see Video 1 in the Supplemental Materials [39]). Although we divided regime I into these two subregimes (1) and (2), this division is not essential. Regime I is characterized by the single exponential decrease of $\Delta\ell$ [see the fitted red curve in Fig. 3(b)]. This should be compared with regimes II and I in sVPS in Figs. 4(b) and 4(c).

C. Case of strongly viscoelastic phase separation

For sVPS [see Fig. 4(a)], after regime i, composition fluctuations are frozen for a while, where not only $\langle I \rangle$ and $(\langle \Delta I^2 \rangle)^{1/2}$ are kept low [see Fig. 4(b)] but also ℓ and w only slightly decrease with time [Figs. 4(b) and 4(c)]. This frozen state is caused by viscoelastic effects (see below). We refer this time regime continuing until t_0 as "regime ii" (see Appendix 4 b). Only the leftmost image in Fig. 4(a) belongs to this regime. After t_0, macroscopic deformation of the transient gel takes place. The first process, which we call "regime II," is characterized by the exponential decrease of both $\Delta\ell$ and Δw [Fig. 4(d)], the coarsening of the internal domain structure, and the temporal change in the outer shape [more specifically, the aspect ratio, see the lower inset of Fig. 4(d)]. The domain coarsening results in the increase in both $\langle I \rangle$ and $(\langle \Delta I^2 \rangle)^{1/2}$ [see Appendix 4 b and Fig. 4(b)]. This behavior is characteristic of volume shrinking of a transient gel formed in regime ii (see below). Then the second (final) process, which we call regime I, is the same as regime I in sVPS in Figs. 4(b) and 4(c).

wVPS, where the transient gel looses elasticity and comes back to a fluid due to viscoelastic relaxation [Fig. 4(c)].

Here it may be worth explaining the difference in the behavior in wVPS [Fig. 3(b)] and sVPS [Fig. 4(b)] in more detail, since they might look apparently similar. To consider this problem, it is crucial to recognize the following facts: (i) Since $\tau_B > \tau_S$ (see Sec. IV B), the absence of the bulk elasticity automatically means the absence of shear elasticity, and the presence of the latter means the presence of the former. (ii) The volume shrinking is driven by the bulk mechanical stress, while the domain coarsening is allowed when the shear elasticity is absent. Then, for the case of Fig. 3(c), there is little volume shrinking after t_0, whereas the domain coarsening proceeds since $\langle I \rangle$ (green triangles) and $(\langle \Delta I^2 \rangle)^{1/2}$ (blue squares) increase. This indicates that the process after t_0 should be liquid-like and should be identified as regime I, where neither bulk nor shear elasticity is active. For the case of Fig. 4(c), on the other hand, there is significant volume shrinking after t_0. This means that the bulk mechanical stress is operative. However, the domain coarsening proceed as can be seen in the increase in $\langle I \rangle$ and $(\langle \Delta I^2 \rangle)^{1/2}$ [see Fig. 4(b)], indicating the absence of the shear elasticity. Thus, we identify this process as regime II, where bulk elasticity is active but shear elasticity is not.

D. Case of fracture phase separation

For FPS [see Fig. 5(a)], after t_0, i.e., after regimes i and ii (only the leftmost image belongs to this regime), which are the same as in sVPS, there appears a new "regime III," where both bulk and shear stresses are active. In this regime [the second and third images in Fig. 5(a) belong to this regime], $\Delta\ell$ and Δw decrease exponentially with time [Fig. 5(d)] and the outer shape is preserved, i.e., the aspect ratio is constant with time [see the lower inset of Fig. 5(d)] but, unlike regime II, composition fluctuations are kept frozen. The latter fact can be seen from the fact that $\langle I \rangle$ and $(\langle \Delta I^2 \rangle)^{1/2}$ are kept low [Fig. 5(b)], indicating that shear elasticity is active.
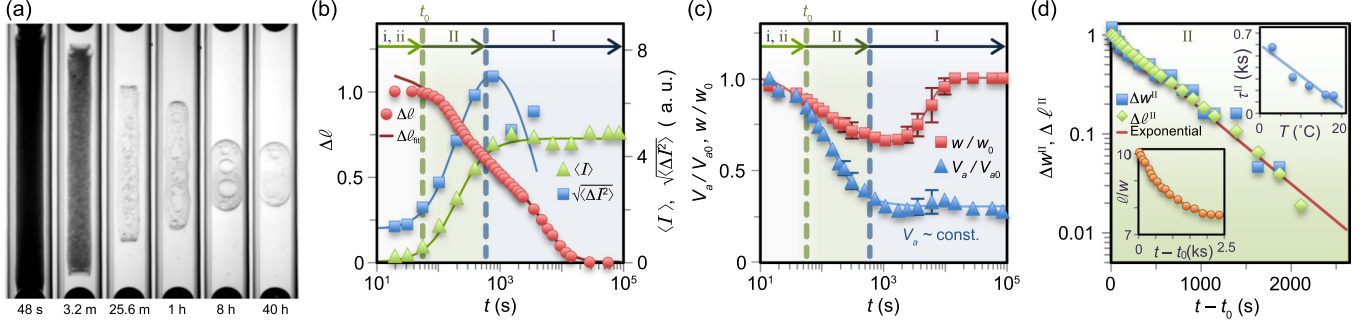
FIG. 4. Volume-shrinking dynamics of a transient gel in sVPS [at 12 °C in panels (a)–(c) and 3 °C in panel (d) for 4 wt% PS1; see Fig. 1(a)]. The descriptions of panels (a)–(c) are the same as in Figs. 3(a)–3(c), respectively. In panel (b), we fit the decay of $\Delta\ell$ by a two-step exponential decay with the two characteristic times, τ^{II} and τ^{I} (see Sec. VI B). See Video 2 in the Supplemental Materials [39] for the shrinking process shown in panel (a). The fluidity of the polymer-rich phase in regime I in sVPS can also be seen in panel (c) from the recovery of w/w_0 due to hydrodynamically driven interface reduction. The slight decrease of the V_a/V_{a0} after 10^4 s comes from the escape of the large DEM-rich droplets encapsulated in the PS-rich phase (see Video 2 in the Supplemental Materials [39]). (d) A process of shape-thickening shrinking in regime II, which is characterized by the same exponential decrease of the $\Delta\ell$ and Δw and also by the decrease in the aspect ratio ℓ/w in the lower inset. The upper inset in panel (d) shows the T dependencies of τ^{II}. Solid lines without legends are to guide the eye.

This suggests that this deformation process is different from regime ii and II (see below). This regime III is followed by regime II and regime I sequentially in this order, as in sVPS. We note that the relaxation time τ^k of the exponential decay of $\Delta\ell$ in each regime k ($k = $ I, II, or III) satisfies the relation of $\tau^I > \tau^{II} > \tau^{III}$ (see Figs. 3–5, and Fig. 12 and Appendix 4 a).

E. Summary

Here we summarize the above-mentioned three types of behavior in Figs. 6(a) and 6(b). Figure 6(a) shows the volume-shrinking behavior induced by phase separation taking place at various temperatures. We can see that, for wVPS taking place between T_c and T_t, the volume-shrinking sequence is regime i → regime I. For sVPS taking place between T_t and T_f, the sequence is regime i → regime ii → regime II → regime I. For FPS taking place below T_f, the sequence is regime i → regime ii → regime III → regime II → regime I. Below T_t but above T_f, only the bulk modulus of a transient gel, K_{tg}, plays a crucial role in its volume-shrinking behavior

whereas, below T_f, the shear modulus μ_{tg} also plays a pivotal role in addition to K_{tg} [35]. The details will be discussed later.

Next we summarize the volume-shrinking behavior shown in Fig. 6(a) in terms of the strain defined as $-\gamma_\ell = (\ell - \ell_0)/\ell_0$ rather than time in Fig. 6(b). The strain $-\gamma_\ell$ is a measure of the degree of volume shrinking and a monotonically increasing function of time. We plot the final strain values in regime III and those in regime II, which provide the border (red curve) between regimes III and II and the border (green curve) between regimes II and I, respectively. Regime I, II, and III are shown by light blue, light green, and light red, respectively. We can see that regimes ii and II appear only below the onset temperature of sVPS, T_t, whereas regime III appears only below the onset temperature of FPS, T_f.

IV. UNIQUE FEATURES OF TRANSIENT GELS

Before making a theoretical description of the volume-shrinking kinetics of a transient gel, we need to clarify the
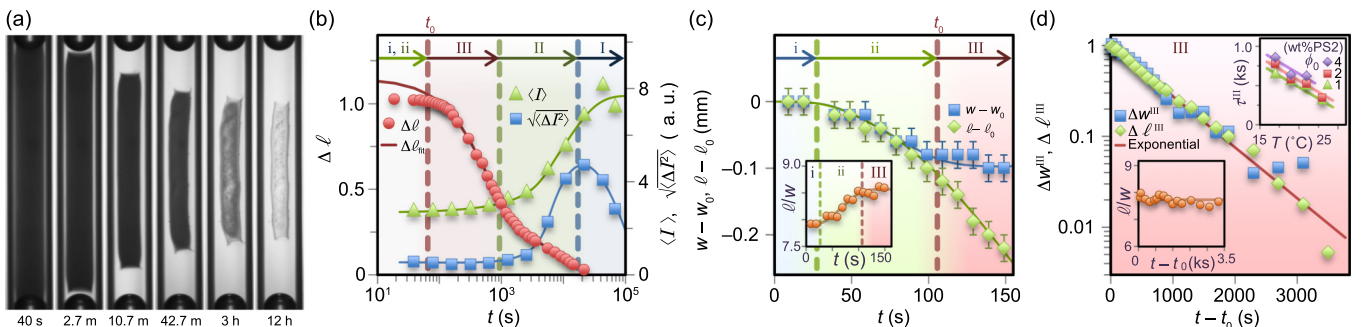

FIG. 5. Volume-shrinking dynamics of a transient gel in FPS [at 19 °C for 1 wt% PS2 in panels (a)–(c) and at 17 °C for 2 wt% PS2 in panel (d); see Fig. 1(b)]. The descriptions of panels (a) and (b) are the same as in Figs. 3(a) and 3(b), respectively. See Video 3 in the Supplemental Materials [39] for the shrinking process in panel (a). (c) An isotropic (or up-hill-diffusion-like) shrinking process in regime ii characterized by the same decrease of $w - w_0$ and $\ell - \ell_0$ (see Sec. VI B). The lower inset in panel (c) demonstrates the temporal change in the aspect ratio ℓ/w characterizing the shrinking process of shape thinning in regime ii. (d) A process of shape-preserving shrinking in regime III, which is characterized by the same exponential decrease of the $\Delta\ell$ and Δw but the constant aspect ratio ℓ/w in the lower inset (in contrast with the lower inset of Fig. 4(d); see also Sec. VI B for more details). The upper inset in panel (d) shows the T dependencies of τ^{III}. Solid lines without legends are to guide the eye.
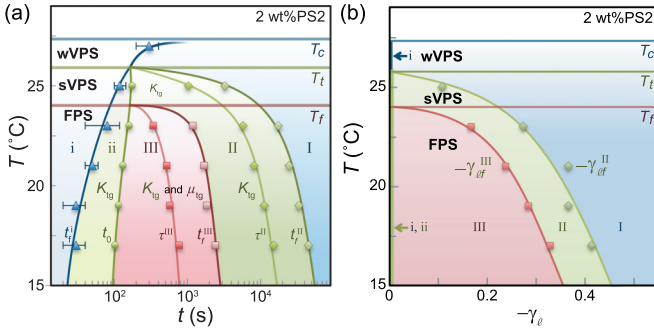
FIG. 6. Summary of phase-separation behavior of PS2-DEM mixtures near the critical composition. (a) The experimental results on the transformation between various time regimes as a function of T for PS2 ($\phi_0 = 2$ wt%). The notation t_f^{III} and t_f^{II} denote the terminal times of regimes III and II, respectively (see Appendix 4 a). τ^{III} and τ^{II} are the characteristic relaxation times of regimes III and II, respectively (see text). We determine the short- and long-time sides of the error bars of the terminal time of regime i, t_f^i, to be respectively the terminal time just before isotropic shrinking starts in regime ii and the starting time of the macroscopic shrinking (their midpoints are represented by triangles) (see Appendix 4 a). We also show the type of elasticity that is active in each process by the labels K_{tg} (bulk modulus) and μ_{tg} (shear modulus). (b) Temperature dependence of the characteristic regimes measured by the degree of strain $-\gamma_\ell$. Here the behavior in panel (a) is shown as a function of the strain rather than time. The strain associated with $\ell(t)$, $-\gamma_\ell$, is obtained as $-[\ell(t) - \ell_0]/\ell_0$. The final strains at $\ell(t) = \ell_f$, $-\gamma_{\ell f}$, were measured for 2 wt% PS2 ($\sim\phi_c$) (see Appendix 4 a). Both $\gamma_{\ell f}^{\mathrm{III}}$ and $\gamma_{\ell f}^{\mathrm{II}}$ in regimes III and II are defined by those at the terminal times t_f^{III} and t_f^{II}, respectively. Solid curves are to guide the eye. The horizontal solid lines show the three key temperatures T_c, T_t, and T_f for 2 wt% PS2 [see Fig. 1(b)].

basic physical nature of a transient gel, which exhibits mechanical relaxation towards a liquid unlike a permanent gel. Here we consider this fundamental problem on a qualitative level.

A. Hierarchical structure formation

It is natural to assume that the early-stage structure formation upon demixing takes place from a shorter to a longer length scale sequentially as time proceeds. The first step of phase separation right after a temperature quench should be collapsing of polymer chains to form "globules," i.e., the coil-to-globule transition induced by a change of the solvent quality from good to poor [33]. Then, in the next step these globules form a transient gel network due to van der Waals attractions between them with a help of hydrodynamic interactions [1,2,40,41]. This process should be essentially the same as transient gelation of colloidal suspensions (or protein solutions) since globules can be regarded as solid-like elastic balls [1,2,6,40–49].

B. Relaxational nature of a transient gel network

Unlike a permanent gel, which has static elasticity coming from a permanent network topology, a transient gel, whose network is formed by transient energetic bonds, does not have static elasticity and its elasticity decays with time: viscoelastic relaxation. There are two types of mechanical relaxation modes, one of which is associated with the volume deformation of a transient gel and the other with its shear deformation. Here it should be noted that the volume deformation of a transient gel inevitably is accompanied by the transport of a liquid whereas its shear deformation does not. Because of this, the volume relaxation time τ_{B} should be much longer than τ_{S} in general: $\tau_{\mathrm{B}} > \tau_{\mathrm{S}}$.

Whether a transient gel behaves like solid or liquid for volume and shear deformation is determined by the relationship between the characteristic mechanical relaxation times for volume and shear deformation, τ_{B} and τ_{S}, respectively, and the characteristic time of the network deformation τ_d. Elastic and liquid-like responses to volume deformation should be observed for $\tau_{\mathrm{B}} \gg \tau_d$ and $\tau_{\mathrm{B}} \ll \tau_d$, respectively. Then, similarly, elastic and liquid-like responses to shear deformation should be observed for $\tau_{\mathrm{B}} > \tau_{\mathrm{S}} \gg \tau_d$ and $\tau_d \gg \tau_{\mathrm{B}} > \tau_{\mathrm{S}}$, respectively.

C. Dynamical crossover and order-parameter switching

To understand the action of mechanical stresses during phase demixing, the key is the time relation of τ_d to τ_{B} and τ_{S} [1,2], which tells us the relevance or irrelevance of bulk and shear elasticity, respectively. In the initial stage of phase separation, τ_d rapidly decreases with time, reflecting the increase of the domain deformation rate, or velocity fields, induced by the growth of the composition gradient, whereas τ_{B} and τ_{S} increase due to the increase in the local polymer composition (see above). In the late stage, on the other hand, the system gradually approaches the equilibrium. Thus, τ_d increases indefinitely, reflecting the slowing down of domain deformation, whereas τ_{B} and τ_{S} saturate to the relaxation times of the equilibrium polymer-rich phase. Thus, τ_d can become shorter than τ_{B} and τ_{S} in the initial stage but becomes longer in the late stage [Figs. 7(a)–7(c)]. Under the constraint of the relation $\tau_{\mathrm{S}} < \tau_{\mathrm{B}}$, which always holds (see above), thus, the following three situations can be realized:

(A) $\tau_{\mathrm{S}} < \tau_{\mathrm{B}} \ll \tau_d$: In this case, the system behaves like a fluid, and thus there is no volume change of the polymer-rich phase. This corresponds to regimes i and I [Fig. 7(a)]. A typical example can be seen in Fig. 3.

(B) $\tau_{\mathrm{S}} \ll \tau_d \ll \tau_{\mathrm{B}}$: In this case, the system has only K_{tg} and no μ_{tg}, i.e., behaves like a solid only for volume deformation but like a fluid for shear deformation. Accordingly, it changes its volume but does not preserve its shape [regimes ii and II; Figs. 7(b) and 7(c)]. A typical example can be seen in Fig. 4.

(C) $\tau_d \ll \tau_{\mathrm{S}} < \tau_{\mathrm{B}}$: In this case, the system has both K_{tg} and μ_{tg} and thus behaves like a solid for both volume and shear deformation. Thus, it changes its volume while preserving its shape [28] [regime III; Fig. 7(c)]. A typical example can be seen in Fig. 5.

This consideration leads to the following identification of the relevant order parameter for each regime. In case (A), the order parameter should be the polymer composition ϕ as in ordinary phase separation [3], and the composition diffusion is the relevant transport mechanism. In cases (B) and (C), on the other hand, the order parameter should be
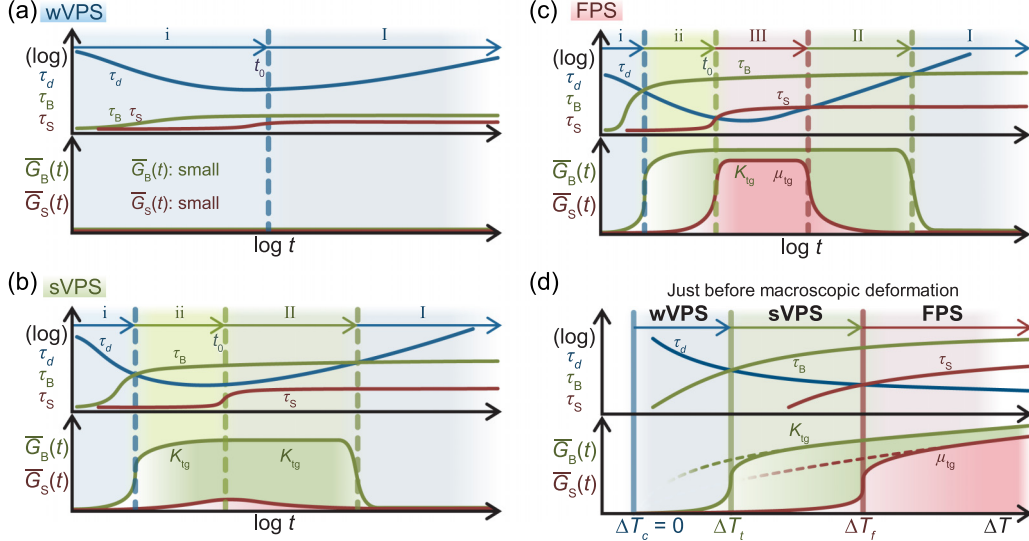
FIG. 7. Characteristic regimes and their sequence during phase separation. Panels (a)–(c) show schematic diagrams of both characteristic times (the top of each) and relaxation moduli (the bottom of each) for wVPS, sVPS, and FPS, respectively. Their ΔT dependencies are schematically shown in panel (d). The bulk and shear relaxation modulus of a transient gel, $\overline{G}_B$ and $\overline{G}_S$, are the volume-averaged ones. The dotted lines in panel (d) denote K_{tg} and μ_{tg}, which are respectively extrapolated from the solid lines of the relaxed $\overline{G}_B$ and $\overline{G}_S$. All the curves are schematic representations of the behavior inferred from our theory.

the deformation tensors (bulk and shear): $d_{ij}^B = \nabla \cdot \mathbf{u}_p \delta_{ij}$ and $d_{ij}^S = \partial u_p^j/\partial x_i + \partial u_p^i/\partial x_j - \frac{2}{3}\nabla \cdot \mathbf{u}_p \delta_{ij}$, respectively, where $\mathbf{u}_p$ is the deformation vector. This means that, during VPS, the order parameter should switch its nature (see below), reflecting the time crossovers [1,2].

V. TWO-FLUID MODEL DESCRIPTION OF VOLUME-SHRINKING KINETICS

On the basis of the above physical picture, we construct a theory that describes the volume-shrinking kinetics of transient gels undergoing phase separation, putting a focus on the linear regime. The key is to incorporate volume and shear deformation "independently" in the framework of a phenomenological two-fluid model [1–3,50]. Since we have to treat rheological properties in a thermodynamically unstable state, we cannot rely on microscopic rheological theories, all of which have been developed to describe a stable state. Thus, we develop a theory based on a phenomenological, but physically relevant argument.

The basic equations of viscoelastic phase separation (VPS) in polymer solutions are expressed by the viscoelastic model [1–3,50] as follows:

$$\frac{\partial \phi}{\partial t} = -\nabla \cdot (\phi \mathbf{v}_p), \tag{1}$$

$$\mathbf{v}_p - \mathbf{v}_s = -\frac{1-\phi}{\zeta}(\nabla \cdot \mathbf{\Pi} - \nabla \cdot \boldsymbol{\sigma}_p), \tag{2}$$

$$\rho \frac{\partial \mathbf{v}}{\partial t} \cong -\nabla \cdot \mathbf{\Pi} + \nabla P + \nabla \cdot \boldsymbol{\sigma}_p, \tag{3}$$

where $\phi = \phi(\mathbf{r}, t)$ is the polymer composition as a function of the position $\mathbf{r}$ and time t, ζ is the friction constant, and ρ is the density. Here $\mathbf{v}_p$ and $\mathbf{v}_s$ are the average velocities of polymer and solvent, respectively, the volume-averaged velocity

$\mathbf{v} = \phi \mathbf{v}_p + (1 - \phi)\mathbf{v}_s$, which satisfies the incompressible condition $\nabla \cdot \mathbf{v} = 0$. P is a part of the pressure and is determined to satisfy the incompressible condition $\nabla \cdot \mathbf{v} = 0$. $\mathbf{\Pi}$ is the osmotic stress tensor given by

$$\nabla \cdot \mathbf{\Pi} = \phi \nabla(\delta \mathcal{F}/\delta \phi),$$

where $\mathcal{F}$ is the Ginzburg–Landau free energy of a mixture, which is given as

$$\mathcal{F} = \int d\mathbf{r}[f_{FH}(\phi(\mathbf{r})) + (C/2)|\nabla \phi(\mathbf{r})|^2],$$

where C is a positive constant. $f_{FH}(\phi(\mathbf{r}))$ is the Flory–Huggins-type free energy per unit volume of the mixture [33]:

$$f_{FH}(\phi, T) = k_B T[(1/N)\phi \ln \phi + (1 - \phi)\ln(1 - \phi)]$$
$$+ \chi(T)\phi(1 - \phi),$$

where k_B is the Boltzmann constant and χ is the Flory's interaction parameter. Then, $\boldsymbol{\sigma}_p$ is the mechanical stress tensor for polymers. For simplicity, we employ the following Maxwell-type constitutive equation to describe the time evolution of $\boldsymbol{\sigma}_p$ [1,2]:

$$\sigma_p^{ij}(t) = \int_{-\infty}^{t} dt' \Big\{ G_S(t - t')\kappa_p^{ij}(t')$$
$$+ G_B(t - t')[\nabla \cdot \mathbf{v}_p(t')]\delta_{ij} \Big\}, \tag{4}$$

where $\kappa_p^{ij}(t) = \partial v_p^j(t)/\partial x_i + \partial v_p^i(t)/\partial x_j - 2/3[\nabla \cdot \mathbf{v}_p(t)]\delta_{ij}$. Here $G_S(t)$ and $G_B(t)$ are the relaxational shear and bulk modulus given respectively by

$$G_S(t) = \mu_{tg}\exp\left(-\frac{t}{\tau_S}\right), \quad G_B(t) = K_{tg}\exp\left(-\frac{t}{\tau_B}\right), \tag{5}$$

where μ_{tg} and K_{tg} are respectively the elastic plateau modulus for shear and bulk deformation and τ_S and τ_B are respectively

the shear and bulk stress relaxation time. In general, the quantities μ_{tg}, K_{tg}, τ_S, and τ_B, are functions of $\phi(\mathbf{r}, t)$. Here, however, we use these values as the volume-averaged ones that depend only on time.

A. Linear theory for a transient gel

We linearize Eq. (1) with respect to the composition fluctuations, $\delta\phi(\mathbf{r}, t) = \phi(\mathbf{r}, t) - \phi_0$, including effects of both the bulk and shear stress in a polymer solution through Eqs. (2)–(5). We also assume $\delta\phi \cong -\phi_0\nabla \cdot \mathbf{u}_p$ [51], where $\mathbf{u}_p$ is the deformation vector of a transient gel and $\partial\mathbf{u}_p/\partial t = \mathbf{v}_p$. Then we obtain the following expression in the wave number (q) space of this linearized equation:

$$\frac{\partial}{\partial t}\phi_q(t) = -\Gamma_q\phi_q(t) - (1-\phi_0)^2\frac{q^2}{\zeta}$$
$$\times \left[K_{tg}\int_{-\infty}^{t} dt' \exp\left(-\frac{t-t'}{\tau_B}\right)\frac{\partial}{\partial t'}\phi_q(t')\right.$$
$$\left. + \frac{4}{3}\mu_{tg}\int_{-\infty}^{t} dt' \exp\left(-\frac{t-t'}{\tau_S}\right)\frac{\partial}{\partial t'}\phi_q(t')\right], \quad (6)$$

where $\Gamma_q = (1-\phi_0)^2 q^2(-|K_{os}| + C\phi_0^2 q^2)/\zeta$ is the growth rate in the absence of viscoelastic effects and $K_{os} = \phi_0^2(\partial^2 f/\partial\phi^2)$ is the osmotic modulus. For simplicity, we assume that in Eq. (6) K_{tg}, μ_{tg}, τ_B, and τ_S are time independent in each regime, or that the major change takes place in the boundary between the regimes [Figs. 7(a)–7(c)].

First we consider regime i, which appears immediately after quenching. It is characterized by a transient globule network with small values of τ_B and τ_S, which satisfy relation (A), or $\tau_d \gg \tau_j$ ($j = $ S or B). The order parameter governing this process is ϕ since elasticity does not play a role in phase separation. For regime i, we can thus approximate the integrals in Eq. (6) by $\tau_j\partial\phi_q(t)/\partial t$. Here we introduce the viscoelastic lengths for bulk and shear deformation as ξ_B and ξ_S, respectively. Following the definition of ξ_S [1,2,50,51], we also define ξ_B as follows:

$$\xi_S^2 = (1-\phi_0)^2\frac{\frac{4}{3}\mu_{tg}}{\zeta}\tau_S, \quad \xi_B^2 = (1-\phi_0)^2\frac{K_{tg}}{\zeta}\tau_B. \quad (7)$$

Then, the linear theory for VPS [51] tells us that the composition fluctuations $\delta\phi = \phi - \phi_0$ obeys the following equation:

$$\left[1 + (\xi_B^2 + \xi_S^2)\nabla^2\right]\frac{\partial\delta\phi}{\partial t}$$
$$= -\frac{(1-\phi_0)^2}{\zeta}\left(-|K_{os}| - C\phi_0^2\nabla^2\right)\nabla^2\delta\phi. \quad (8)$$

By rewriting Eq. (6) as $\partial\phi_q(t)/\partial t = -\Gamma_{eff}^i\phi_q(t)$, we obtain the growth rate including viscoelastic effects of a transient gel, Γ_{eff}^i, for regime i [i.e., Eq. (1)]:

$$\Gamma_{eff}^i = \frac{\Gamma_q}{1 + (\xi_B^2 + \xi_S^2)q^2}$$
$$= (1-\phi_0)^2\frac{q^2}{\zeta}\frac{-|K_{os}| + C\phi_0^2 q^2}{1 + (\xi_B^2 + \xi_S^2)q^2} < 0, \quad (9)$$

where $-\Gamma_q$ is the growth rate in the absence of viscoelastic effects. Note that the negative sign of Γ_{eff}^i means the growth of $\delta\phi$.

Next we consider regimes ii and III, where elasticity plays a crucial role, or the order parameter is d_{ij}. For convenience, we use $\mathbf{u}_p$ as a key variable rather than d_{ij}, as in the case of a permanent gel [24–31]. Using $\delta\phi \cong -\phi_0\nabla \cdot \mathbf{u}_p$ [51] [Eq. (1)] with Eqs. (4) and (5), we obtain the following linearized equation for $\mathbf{u}_p$ from Eq. (2):

$$\frac{\partial}{\partial t}\mathbf{u}_p(t) - \mathbf{v}_s$$
$$= \frac{1-\phi_0}{\zeta}\left\{-|K_{os}|\nabla\nabla \cdot \mathbf{u}_p(t) + C\phi_0^2\nabla^2\nabla\nabla \cdot \mathbf{u}_p(t)\right.$$
$$+ \left[K_{tg}\int_{-\infty}^{t} dt' \exp\left(-\frac{t-t'}{\tau_B}\right)\frac{\partial}{\partial t'}\nabla\nabla \cdot \mathbf{u}_p(t')\right.$$
$$+ \mu_{tg}\int_{-\infty}^{t} dt' \exp\left(-\frac{t-t'}{\tau_S}\right)$$
$$\left.\left. \times \frac{\partial}{\partial t'}\left(\frac{1}{3}\nabla\nabla \cdot \mathbf{u}_p(t') + \nabla^2\mathbf{u}_p(t')\right)\right]\right\}. \quad (10)$$

Hereafter we use the long-wavelength-limit approximation to obtain the solution for surface deformations and also the relation $\nabla\nabla \cdot \mathbf{u}_p = \nabla^2\mathbf{u}_p$ from the fact that $\nabla \times \nabla \times \mathbf{u}_p = \mathbf{0}$ for the cylindrical geometry [28]. In this limit, the shear stress term ($\sim\xi_S^2\nabla^2\partial\mathbf{u}_p/\partial t$) in Eq. (10) can be ignored [since $\xi_S \ll r_0$, where r_0 ($=w_0/2$) is the initial radius of the cylinder].

For regime ii where $\tau_B \gg \tau_d \gg \tau_S$, we can approximate the integrals in Eq. (10) by $\nabla\nabla \cdot \mathbf{u}_p$ for bulk stress (the third term on the right hand side) and by $\tau_S\partial/\partial t\nabla\nabla \cdot \mathbf{u}_p$ for shear stress (the fourth term). Furthermore, we can assume $\mathbf{v}_s \sim -[\phi_0/(1-\phi_0)]\partial\mathbf{u}_p/\partial t$ since $\mathbf{v} \sim \mathbf{0}$ in regime ii, where the motion of a transient gel is purely diffusive since there is no shear elasticity. Then, the time development of $\mathbf{u}_p$ can be described in the long-wavelength limit (see above) by the following diffusion-type equation,

$$\frac{\partial\mathbf{u}_p}{\partial t} = \frac{(1-\phi_0)^2}{\zeta}(\nabla \cdot \boldsymbol{\sigma}_p - \nabla \cdot \boldsymbol{\Pi})$$
$$\simeq \frac{(1-\phi_0)^2}{\zeta}(K_{tg} - |K_{os}|)\nabla^2\mathbf{u}_p. \quad (11)$$

The characteristic decay time is thus given by Eq. (2):

$$\tau^{ii} = \frac{r_0^2}{(1-\phi_0)^2}\frac{\zeta}{K_{tg} - |K_{os}|} > 0, \quad (12)$$

where r_0 ($=w_0/2$) is the radius of the cylinder. In regime ii, the mechanical force density $\nabla \cdot \boldsymbol{\sigma}_p = K_{tg}\nabla^2\mathbf{u}_p$ (from bulk stress in this case) should overwhelm the osmotic one $\nabla \cdot \boldsymbol{\Pi} = |K_{os}|\nabla^2\mathbf{u}_p$. This situation is expressed by the relation (a) $K_{tg} > |K_{os}|$. This relation $\nabla \cdot \boldsymbol{\sigma}_p > \nabla \cdot \boldsymbol{\Pi}$ means that the spontaneous shrinking is the result of mechanical stabilization of the thermodynamically unstable system ($K_{os} < 0$) by self-generated stress. Note that this situation is the same in regime III, as shown later.

For regime III where τ_B, $\tau_S \gg \tau_d$, on the other hand, we approximate the integrals by $\nabla\nabla \cdot \mathbf{u}_p$ for both stresses. In this regime, thus, we have the following equation of motion for $\mathbf{u}_p$

in the long-wavelength limit (see above), which is identical to the one describing a permanent gel [24,25,28–31]:

$$\frac{\partial \mathbf{u}_p}{\partial t} - \mathbf{v}_s = \frac{1-\phi_0}{\zeta}\left(K_{\mathrm{tg}} + \frac{4}{3}\mu_{\mathrm{tg}} - |K_{\mathrm{os}}|\right)\nabla^2\mathbf{u}_p, \quad (13)$$

where $\mathbf{v}_s$ is the local solvent velocity. Regime III appears when $\nabla \cdot \boldsymbol{\sigma}_p > \nabla \cdot \boldsymbol{\Pi}$ as the same as regime ii. However, since $\nabla \cdot \boldsymbol{\sigma}_p = (K_{\mathrm{tg}} + \frac{4}{3}\mu_{\mathrm{tg}})\nabla^2\mathbf{u}_p$, we also need relation (b) $K_{\mathrm{tg}} + \frac{4}{3}\mu_{\mathrm{tg}} > |K_{\mathrm{os}}|$ in addition to the above relation (a) $K_{\mathrm{tg}} > |K_{\mathrm{os}}|$. Following Refs. [24,25,28–31], we derive a special solution with relation (c) $K_{\mathrm{tg}} - |K_{\mathrm{os}}| \ll \frac{4}{3}\mu_{\mathrm{tg}}$ (see below and Sec. VI B 3): $\Delta\ell^{\mathrm{III}}(t) = \Delta w^{\mathrm{III}}(t) = \exp(-t/\tau^{\mathrm{III}})$ and constant ℓ/w, implying "shape-preserving" shrinking. Here τ^{III} is the characteristic time of shrinking given by Eq. (3):

$$\tau^{\mathrm{III}} = \frac{r_0^2}{a^{\mathrm{III}}(1-\phi_0)}\frac{\zeta}{K_{\mathrm{tg}} + \frac{4}{3}\mu_{\mathrm{tg}} - |K_{\mathrm{os}}|} > 0, \qquad (14)$$

where a^{III} is a positive constant. This solution explains our results shown in Fig. 5(d) with its lower inset and in Fig. 13(a).

These equations for regimes ii and III are essentially the same in their mathematical structures as the equations of motion of a permanent gel, and thus we can solve them by the method described in Refs. [28–31], under the stress-free boundary condition. The solution for regime ii in the absence of shear elasticity is obtained as $\Delta w^{\mathrm{ii}}(t) = \sum_{n=1}^{\infty} B_n \exp(-t/\tau_n^{\mathrm{ii}})$ with the relation for the characteristic decay time in regime ii, $\tau^{\mathrm{ii}} = a_n^{\mathrm{ii}}\tau_n^{\mathrm{ii}}$ [see Eq. (12)]. Here τ_n^{ii} is the nth decay time, and a_n^{ii} is a positive constant determined by the boundary condition, and the coefficient B_n is determined by the initial condition. The solution for regime III is, on the other hand, obtained as $\Delta\ell^{\mathrm{III}}(t) = \Delta w^{\mathrm{III}}(t) = \exp(-t/\tau^{\mathrm{III}})$ with the characteristic decay time in regime III, τ^{III} [see Eq. (14)]. The positive constant a^{III} in Eq. (14) is determined by the stress-free boundary condition as a function of the moduli [28,30,31] ($a^{\mathrm{III}} \lesssim 1$ in our case). Here we briefly discuss the meaning of these τ^{ii} and τ^{III} and the origin of the transient gel shrinking. The osmotic part of their denominators in Eqs. (12) and (14) ($|K_{\mathrm{os}}|$) indicates the driving force of phase separation, or deformation, of a transient gel. The elastic parts of their denominators [K_{tg} in Eq. (12) and $K_{\mathrm{tg}} + \frac{4}{3}\mu_{\mathrm{tg}}$ in Eq. (14)] indicates elastic registing force for the deformation. Thus, the denominators (with positive values) represent restoring force in the shrinking process: a transient gel shrinks by the restoring force. The numerators of these characteristic times means friction force for the relative motion between a polymer network and solvent. Therefore, these characteristic times depend on the ratio of the friction force in the numerators and the restoring force in the denominators.

We obtain relation (a) for regime ii and relations (a) and (b) for regime III from the stable shrinking condition (τ^{ii}, $\tau^{\mathrm{III}} > 0$) as well as the consistency with the freezing of the inner structure. We exclude the case where both $K_{\mathrm{tg}} < |K_{\mathrm{os}}|$ [the opposite of relation (a)] and relation (b) are satisfied, since this case corresponds to "macroscopic instability" [29,51]. We obtain relation (c) from the fact that the decays of $\Delta\ell(t)$ and $\Delta w(t)$ are both described by single exponential decays [Fig. 5(d)] (see the calculation in Refs. [28,30]). We note that for the opposite case of relation (c) seen in a permanent gel we should see multiple exponential decays [28,30,31].

Finally we consider the temporal change in the compositional field in regime ii and III, where elasticity plays a dominant role. The decay rate of ϕ_q for regime ii, $\Gamma_{\mathrm{eff}}^{\mathrm{ii}}$, and that for regime III, $\Gamma_{\mathrm{eff}}^{\mathrm{III}}$, are obtained as follows: by applying the same approximation to the integrals in Eq. (10) for each regime as to Eq. (6):

$$\Gamma_{\mathrm{eff}}^{\mathrm{ii}} = (1-\phi_0)^2\frac{q^2}{\zeta}\frac{K_{\mathrm{tg}} - |K_{\mathrm{os}}| + C\phi_0^2 q^2}{1 + \xi_S^2 q^2} > 0, \qquad (15)$$

$$\Gamma_{\mathrm{eff}}^{\mathrm{III}} = (1-\phi_0)^2\frac{q^2}{\zeta}\left(K_{\mathrm{tg}} + \frac{4}{3}\mu_{\mathrm{tg}} - |K_{\mathrm{os}}| + C\phi_0^2 q^2\right) > 0. \qquad (16)$$

These results indicate the decay of the composition fluctuations for all q, i.e., phase separation proceeds in the form of volume shrinking of a transient gel without the growth of composition fluctuations. The apparent freezing of the coarsening of "inner structure" observed in these regimes indicates that the slow decay of $\delta\phi$, and thus that $K_{\mathrm{tg}} - |K_{\mathrm{os}}|$ should be small.

B. Justification of the linearization with respect to composition fluctuations for regimes ii and III

Here we consider how the linearization of the theory with respect to composition fluctuations can be justified for regimes ii and III. What is important is that, even though $K_{\mathrm{os}} < 0$ in the unstable state, the elastic nature of a transient gel leads to the situation $K_{\mathrm{tg}} - |K_{\mathrm{os}}| > 0$ for regime ii and $K_{\mathrm{tg}} + 4\mu_{\mathrm{tg}}/3 - |K_{\mathrm{os}}| > 0$ for regime III, which suppresses the growth of the composition fluctuations. Thus, as long as a transient gel behaves as an elastic network, the mechanics rather than thermodynamics dominates the behavior for regimes ii and III: Macroscopic volume deformation takes place while the growth of the composition fluctuations being suppressed. This allows us to treat the process as a linear regime with respect to the composition fluctuations as in Eq. (6), even when macroscopic volume change takes place. This argument can also be justified by the following fact: The linear approximation provides us with Eq. (13), which is the same for the equation describing the volume shrinking of a permanent chemical gel, and this equation can indeed describe the experimentally observed volume-shrinking processes in regimes ii and III. Thus, we argue that we may treat not only regime I, but also regimes ii and III as the linear regime with respect to the composition fluctuations. On the other hand, regime II should be treated as a nonlinear process because the coarsening of internal structures takes place due to the relaxation of the shear stress. Furthermore, regime I corresponds to the ordinary nonlinear late stage of phase separation since both bulk and shear stresses are already relaxed.

VI. DISCUSSION

On the basis of the above theory, we now explain our experimental results on the volume-shrinking dynamics of a transient gel during phase separation in more detail.

A. Physical nature of transient globule network

In the above we show that the transient nature of a globule network plays a crucial role in understanding a transient gel state. Here we consider its physical nature in more detail. First we estimated the friction constant ζ from $\zeta \sim 6\pi\eta_0\phi_0^2/b^2$ [51], where we regard b as the globule diameter and η_0 is the solvent viscosity. We approximate the value of b to be of the order of 10 nm [52], although it should depend on the quench condition, the molecular weight of polymers, and the number of polymer chains involved in a globule. Under these assumptions, we obtain $\zeta \sim 10^{10}$ Pa s/m^2 for $\eta_0 \sim 2$ mPa s (for DEM) and $\phi_0 \sim 0.01$. Next, inserting this value of ζ and $\tau^{\mathrm{III}} \sim 10^3$ s [the upper inset in Fig. 5(d)] into Eq. (14), we obtain $K_{\mathrm{tg}} - |K_{\mathrm{os}}| + \frac{4}{3}\mu_{\mathrm{tg}} \sim 1$ Pa. In our case, $K_{\mathrm{tg}} - |K_{\mathrm{os}}| \sim 0.1\mu_{\mathrm{tg}}$ [28], and thus we obtain $\mu_{\mathrm{tg}} \sim 1$ Pa. We speculate that $K_{\mathrm{tg}} \sim |K_{\mathrm{os}}| \sim \mu_{\mathrm{tg}}$. We note that these values of ζ and μ_{tg} are many orders of magnitude smaller than those of a permanent gel ($\zeta = 10^{12} \sim 10^{14}$ Pa s/m^2 and $\mu = 10 \sim 10^3$ Pa [24,25,28,29]). This is a direct consequence of a much larger mesh size of the transient network than the chemical gel network; for example, the elastic moduli scales as λ^{-3} [3,7], where λ is the pore size, or the characteristic length of network strands. Note that λ should be roughly proportional to the characteristic size of a strand unit, which is a monomer (or blob [51]) for a permanent gel [24,29] and a globule for a transient gel, when ϕ_0 is similar between the two types of gels. Using these values, the above τ^{ii} is roughly estimated as $\tau^{\mathrm{ii}} \sim r_0^2/D^{\mathrm{ii}} \sim 10^4$ s [Eq. (12)], by assuming $r_0 = 0.5$ mm and the diffusion constant in regime ii $D^{\mathrm{ii}} \sim (K_{\mathrm{tg}} - |K_{\mathrm{os}}|)/\zeta \sim 10^{-11}$ m^2/s, which is comparable to the cooperative diffusion constant of polymers in a good solvent [22,53].

Here we list special characteristics of the transient globule network.

(1) The network composed of globules is responsible for the softness of a transient gel (see above).

(2) Interglobule attractions due to the large thermodynamic driving force $|K_{\mathrm{os}}|/\phi_0^2$ [1–3] are the origin for the formation of the connected network. Thus, a transient gel has the elasticity of energetic origin, unlike a permanent gel whose elasticity is of entropic origin [33]. Thus, the elasticity of a transient gel should increase with an increase in ΔT. This can indeed be seen from the fact that a transient gel can keep its shape for large ΔT but not for small ΔT under the action of gravity (Fig. 8). We note that the entropic contribution to a transient gel should be very small because of a much fewer degrees of freedom of a globular state than a coil state of polymer. Finally, the finiteness of the relaxation times τ_{B} and τ_{S} leads to the following very unique features of a transient gel:

(3) The unique relaxational nature of the network under the self-generated mechanical stress is the key to have the relation $\tau_{\mathrm{B}} > \tau_{\mathrm{S}}$, as explained in Sec. IV B. This condition leads to the realization of relations (A)–(C): For relation (A), a transient gel without elasticity (regimes i and I) is realized; for relation (B), a transient gel with only K_{tg} is realized (regimes ii and II); and for relation (C) a transient gel with both K_{tg} and μ_{tg} is realized (regime III). Such independent variations of K_{tg} and μ_{tg} are the characteristics of a transient gel and are not allowed for a permanent gel, where $\tau_{\mathrm{B}}, \tau_{\mathrm{S}} \to \infty$ and thus
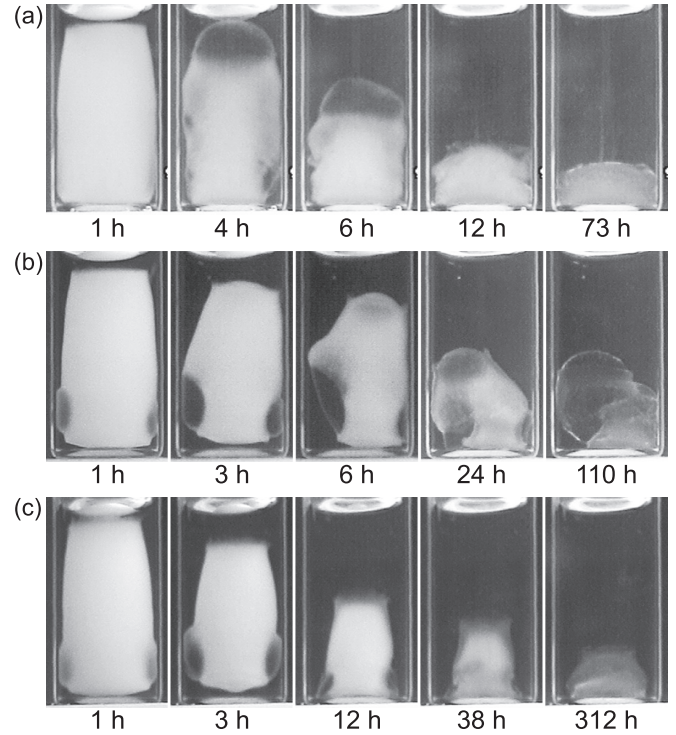

FIG. 8. Shape-preserving effect of shear modulus of transient gels under gravity and its temperature dependence. We show processes of shrinking and collapsing of transient gels under gravity in a glass vial at 2 wt% PS2 for three temperatures; (a) at 20 °C, (b) at 16 °C, and (c) at 12.6 °C. In this experiment, a sample vial containing a solution in a mixed one-phase state was immersed into a water bath whose temperature is controlled at a target temperature. Here the reflected light image of the process was captured by a CCD camera and, thus, a phase-separated transient gel was observed as a bright white object, unlike the above back-illuminated image, where it appears as a dark object. For a lower temperature, the speed of the collapsing is slower because of the larger shear modulus of transient gels, which also strengthens the shape-preserving ability during shrinking. "Voids" in top and bottom of these transient gels may be formed by mechanical instability characteristic of shrinking under gravity. We note that similar instability, or bubble formation, was observed in a volume shrinking of a chemically cross linked permanent gel [27].

both static bulk and shear moduli (K and μ respectively) of the permanent gel are strongly correlated.

B. Characteristic features of each regime

In the following, we consider the characteristic features of regimes i, ii, III, II, and I one by one in more detail.

1. Regime i

Regime i appears immediately after a quench for all of wVPS, sVPS, and FPS: This is the process before forming a transient globule network by random connection between globules, and characterized by short τ_{B} and τ_{S}, which satisfy relation (A). We note that, for the PS-DEM mixtures, the onset temperature of sVPS, T_t, has a maximum at a composition ϕ_t slightly lower than the critical composition ϕ_c [34] [Figs. 1(a)

and 1(b)]. The appearance of sVPS at ϕ_t even for a very shallow quench indicates that in the unstable region of $\phi_0 > \phi_t$ the transient connectivity of a globule network is realized in the early stage of VPS. However, the appearance of wVPS near ϕ_c indicates that viscoelastic effects appear even in regime i. In regime i, $\delta\phi$ can grow in the characteristic length scale beyond the viscoelastic lengths, ξ_B and ξ_S, which are rather short there.

The order parameter governing this process is the composition ϕ since elasticity does not play a role in phase separation. The growth rate including viscoelastic effects, $-\Gamma_{eff}^i$, is given by Eq. (9). Note that the negative sign of Γ_{eff}^i means the growth of composition fluctuations, $\delta\phi$. As phase separation proceeds, τ_d decreases, whereas τ_B increases [1,2]. If $\delta\phi$ reaches the equilibrium value before τ_B exceeds τ_d, then regime i is followed by (fluid-like) regime I [wVPS, Fig. 7(a)]. Otherwise, regime i is followed by regime ii.

2. Regime ii

Next we consider regime ii, which appears for sVPS and FPS. Regime ii is characterized by relation (B). A transient network shrinks its whole volume while the internal structure is kept, but cannot keep its outer shape, since it has only bulk elasticity K_{tg} and no shear elasticity μ_{tg}. Thus, it behaves as an elastic body for volume deformation, but as a fluid for shear deformation, resulting in volume shrinking without preserving the shape [note that the aspect ratio changes with time as shown in the lower inset in Fig. 5(c)]. Such a behavior can be seen as "isotropic shrinking" [here, "isotropic shrinking" means the same amount of shrinking in both directions: note that $\ell - \ell_0 \cong w - w_0$ in regime ii; see Fig. 5(c) and its lower inset]. In this regime, the "pure" diffusion-type equation of $\mathbf{u}_p$, Eq. (11), holds and thus the process is similar to *nonlocal* "up-hill diffusion" rather than ordinary *local* mechanical relaxation. Although the volume-shrinking process takes place through the side surface of a cylindrical gel as well as its both end caps [see Fig. 5(c)], the characteristic lengths of the former and latter are both about the radius of the cylinder r_0. Thus, the characteristic decay times for the two directions are commonly characterized by $\tau^{ii} = r_0^2 \zeta / [(1 - \phi_0)^2 (K_{tg} - |K_{os}|)]$ [Eq. (12)]. This explains the isotropic shrinking (see above for its meaning) seen in Fig. 5(c).

In regime ii, the order parameter is d_{ij}. The characteristic decay time is thus given by Eq. (12). In regime ii, the mechanical force density from bulk stress should overwhelm the osmotic one: (a) $K_{tg} > |K_{os}|$. This relation means that the spontaneous shrinking is the result of mechanical stabilization of the thermodynamically unstable system ($K_{os} < 0$) by self-generated stress (the same occurs in regime III, as shown later). Continuous network reorganization induced by interglobular attractions leads to the increase in the network density. This causes the increase in τ_S, leading to the following bifurcation towards regime II or III: Regime II appears if the network starts to be disconnected before τ_S exceeds τ_d [sVPS, Fig. 7(b)], whereas regime III appears if τ_S exceeds τ_d before the network breakup starts [FPS, Fig. 7(c)].

3. Regime III

Next we consider regime III, which is characterized by relation (C). This means that both shear and bulk elasticity

(μ_{tg} and K_{tg}) are active: the network macroscopically deforms as a permanent gel [1–3,51] while keeping its shape [28]. The characteristic time of shrinking in regime III is given by Eq. (14). This solution explains our results of the exponential decays shown in Fig. 5(d) with its lower inset and in Fig. 13(a). Regime III appears when (a) $K_{tg} > |K_{os}|$ as in regime ii, but we also need relation (b) $K_{tg} + \frac{4}{3}\mu_{tg} > |K_{os}|$. During this permanent-gel-like shrinking, the liquid-type coarsening cannot proceed because of the action of both bulk and shear elasticity. We also have another relation (c) $K_{tg} - |K_{os}| \ll \frac{4}{3}\mu_{tg}$ for a transient gel. This relation is opposite to the relation $K - |K_{os}| \gtrsim \frac{4}{3}\mu$ for a permanent gel having both static bulk and shear modulus, K and μ [28,30]. This is a consequence of the fact that a transient gel is much softer than a permanent gel (see Sec. VI A). As the shrinking process proceeds, ϕ approaches its equilibrium value, leading to the increase of τ_d with time. Thus, τ_d exceeds τ_S again [Fig. 7(c)], which results in the crossover from regime III to regime II.

4. Regime II

Now we consider regime II, which is characterized by relation (B). In this regime, the globule network is mechanically relaxed for shear deformation but still keeps its bulk elasticity, and thus it shrinks further but without the action of shear elasticity. Thus, $\Delta\ell^{II}(t) = \Delta w^{II}(t) = \exp(-t/\tau^{II})$ but ℓ/w decreases with time [see Fig. 4(d) with its lower inset and Fig. 13(b)]. The relaxation time τ^{II} is given by an equation similar to τ^{ii}. However, when τ_d far exceeds τ_S [Figs. 7(b) and 7(c)], the network becomes gradually softer with time. This allows domain coarsening of the inner structure (or fracturing) to take place unlike in regimes ii and III. As the result, τ_d eventually exceeds τ_B [Figs. 7(b) and 7(c)], leading to the crossover from regime II to regime I.

5. Regime I

This final stage, regime I, is characterized by relation (A). In this regime, the fully relaxed network can follow slow deformation by reorganizing its structure; in other words, the polymer-rich phase behaves as a fluid. Upon the crossover from regime II to regime I, thus, the relevant order parameter switches back from d_{ij} to ϕ. Thus, the change of the outer shape of the polymer-rich phase is not driven by mechanical stresses, but by interfacial tension [Figs. 3(c) and 4(c)], as in ordinary fluid phase separation [3].

6. Summary

We can summarize these dynamical crossovers associated with the emergence of a transient gel state and its disappearance as follows (see Table I): In the initial stage the system sequentially acquires elasticity in the order of bulk (from i to ii) and shear (to III) and then in the late stage it looses elasticity in the order of shear (from III to II) and bulk (and to I) [Figs. 7(a)–7(c)]. The experimental results on the temperature dependence are summarized in Fig. 6.

C. Dependence on quench depth

On the basis of the above transient network model, we now provide qualitative explanations for the transitions between

TABLE I. Characterization of various regimes in phase separation.

Symbol	Phenomena	Phase-separation type
i	Spinodal decomposition with a viscoelastic delay	wVPS, sVPS, FPS
ii	"Up-hill-diffusion-like" shrinking with internal structure freezing	sVPS, FPS
III	"Shape-preserving" shrinking with internal structure freezing	FPS
II	"Shape-changing" shrinking with coarsening of internal structure	sVPS, FPS
I	Hydrodynamic coarsening driven by interfacial tension	wVPS, sVPS, FPS

Symbol	Rheological relations	Moduli	Characteristic time
i	Relation (A): $\tau_S < \tau_B \ll \tau_d$		$1/\Gamma^i_{\text{eff}} = \frac{1}{(1-\phi_0)^2 q^2} \frac{\zeta[1+(\xi_B^2+\xi_S^2)q^2]}{-|K_{\text{os}}|+C\phi_0^2 q^2}$
ii	Relation (B): $\tau_S \ll \tau_d \ll \tau_B$	K_{tg}	$\tau^{ii} = \frac{r_0^2}{(1-\phi_0)^2} \frac{\zeta}{K_{\text{tg}}-|K_{\text{os}}|}$
III	Relation (C): $\tau_d \ll \tau_S < \tau_B$	K_{tg} and μ_{tg}	$\tau^{III} = \frac{r_0^2}{a^{III}(1-\phi_0)} \frac{\zeta}{K_{\text{tg}}-|K_{\text{os}}|+\frac{4}{3}\mu_{\text{tg}}}$
II	Relation (B): $\tau_S \ll \tau_d \ll \tau_B$	K_{tg}	$\tau^{II}(\sim \tau^{ii} \sim \frac{\zeta}{K_{\text{tg}}-|K_{\text{os}}|})$
I	Relation (A): $\tau_S < \tau_B \ll \tau_d$		τ^I

Symbol	Stage [1–3,51]	Order parameter
i	Early stage	Polymer composition, ϕ
ii	Early stage	Deformation tensor of a transient gel, d_{ij}
III	Early stage	Deformation tensor of a transient gel, d_{ij}
II	Intermediate stage	Deformation tensor of a transient gel, d_{ij}
I	Late stage	Polymer composition, ϕ

the three types of VPS. First, we explain the ΔT dependence of the transitions [see Figs. 6(a) and 6(b)] by comparing τ_B and τ_S with τ_d when τ_d becomes minimum. An increase in $|K_{\text{os}}|/\phi_0^2$ with ΔT leads to the increase in τ_B and τ_S [the above feature (2)], but to the decrease in τ_d [1,2] [Fig. 7(d)]. Thus, the increase in ΔT induces the crossover between τ_d and τ_B around t_0 [Figs. 7(a)–7(c)]. This realization of relation (B) leads to the emergence of a transient globule network with only K_{tg}, resulting in the change from wVPS [regime i $\rightarrow$ I in Fig. 7(a)] to sVPS [appearance of regime ii and II in Fig. 7(b)]. A further increase in ΔT leads to the crossover between τ_d and τ_S. This realization of relation (C) leads to the emergence of both K_{tg} and μ_{tg}, resulting in the change from sVPS to FPS [appearance of regime III in Fig. 7(c)].

D. Dependence of T_t and T_f on ϕ_0 and N

Next, we explain the dependence of T_t and T_f on ϕ_0 near the critical composition ϕ_c [Figs. 1(a)–1(c) and 9]. Both T_t and T_f decrease with an increase in ϕ_0 [34,35] [Figs. 1(a) and 1(b)]. In other words, the crossover temperature below which τ_d becomes shorter than τ_B and τ_S becomes lower with an increase in ϕ_0. The increase in ϕ_0 should lead to the increase in both τ_B and τ_S, but the increase in τ_d is steeper than these; that is, the phase-separation speed becomes slower more rapidly. Thus, we need a larger quench depth, or a stronger driving force for demixing ($|K_{\text{os}}|/\phi_0^2$), for higher ϕ_0 to induce elastic response to both volume and shear deformation. We note that, for a too low ϕ_0, a transient gel cannot be formed any more and thus phase separation proceeds with droplet morphology [1,2] since the percolation of globules cannot be attained below a certain ϕ_0 [see the dashed dotted curves in the left sides of Figs. 1(a) and 1(b)].

The same arguments can also apply to the polymerization index N dependencies of T_f at ϕ_c, which are shown in Figs. 1(c) and 9. This is because larger N means lower $\phi_0 \sim \phi_c$ [note that ϕ_c depends on N as $\phi_c(N) \sim 1/\sqrt{N}$ [22,33]].
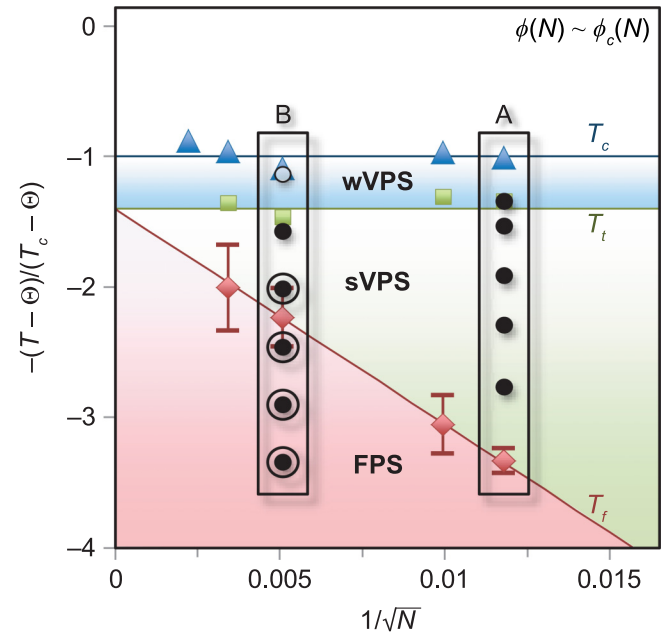

FIG. 9. Dynamical state diagram of critical PS solutions with various degrees of polymerization N. The reduced temperatures $-(T - \Theta)/(T_c - \Theta)$ for the three transition temperatures, T_c, T_t, and T_f, fall onto the straight lines when they are plotted against $1/\sqrt{N}$. The data points for the three transition temperatures are the same as those in Fig. 1(c). State points studied in this work are expressed by the same black symbols as those in Fig. 1(c).

Thus, we may conclude that whether a transient gel behaves elastic or liquid-like for shear deformation is controlled by neither ϕ_0 nor N in a direct manner, but by the crossover between the relevant timescales.

E. Difference in shrinking behavior between a transient and permanent gel

In regime III, we obtain relation (c), $K_{tg} - |K_{os}| \ll \frac{4}{3}\mu_{tg}$, for a transient gel. For a permanent gel, on the other hand, we usually have the following relation opposite to relation (c): $K - |K_{os}| \gtrsim \frac{4}{3}\mu$ [relation (c′)], where K and μ are the bulk and shear modulus, respectively. This difference leads to a crucial difference in the shrinking behavior between the two types of gels.

Below we show that this stems from the difference in the softness between them. First we assume that K_{tg} and μ_{tg} are of the same order, i.e., $K_{tg} \gtrsim \mu_{tg}$ for a transient gel, as in a permanent gel ($K \gtrsim \mu$) [24,25,29]. Then, from relations (c) and (c′), we obtain $K_{tg} - \frac{4}{3}\mu_{tg} \ll K - \frac{4}{3}\mu$, provided that $|K_{os}|$ is of the same order for both cases. This indicates that both K_{tg} and μ_{tg} are much smaller than K and μ. This difference in the softness comes from the difference in the sparseness, reflecting the difference in the unit size between globules for a transient gel and monomers for a permanent gel, as discussed in Sec. VI A.

Next we discuss the different shrinking behaviors of the two types of gels originating from this difference. Relation (c) indicates that the shape-preserving tendency due to the shear modulus μ_{tg} is much stronger than the volume-shrinking tendency due to $K_{tg} - |K_{os}|$ for a transient gel, which is the opposite of relation (c′) for a permanent gel. Since the shape-preserving effect of μ_{tg} tends to minimize shear deformation [28], a transient gel with relation (c) shrinks uniformly. This results in the single exponential decay of its size during shrinking [28,30] [regime III in Fig. 5(d)]. On the other hand, a permanent gel satisfying relation (c′) shrinks in a nonuniform manner, accompanied by the enhancement of composition fluctuations due to a strong driving force towards shrinking, $K - |K_{os}|$ [28], and, thus, the shrinking in the early stage is expressed by the summation of multiple exponentials [25,28,30,31]; more precisely, the outer interface of a gel shrinks faster than its bulk part in a nonuniform manner, but its shape is kept almost the same during the process.

F. Possibility of permanent-gel-like phase separation

Although not yet observed experimentally, we speculate that the increase of the elastic nature of a transient gel with an increase in ΔT might eventually result in an interesting situation below T_f. The increase of $\tau^{III} \propto (K_{tg} + \frac{4}{3}\mu_{tg} - |K_{os}|)^{-1}$ and $\tau^{II} \propto (K_{tg} - |K_{os}|)^{-1}$ with an increase in ΔT [see upper insets of Figs. 5(d) and 4(d) respectively and see also Fig. 10] indicates that K_{tg} and μ_{tg} increase with ΔT more slowly than $|K_{os}|$ does (Fig. 11). Thus, there is a possibility that, below a temperature T_{gel} much lower than T_f, the relation $|K_{os}| > K_{tg} + \frac{4}{3}\mu_{tg}$ is satisfied (Fig. 11). Below T_{gel}, thus, a transient gel should behave as an *unstable* permanent gel, i.e., "gel phase separation" [29,51] ["GPS" below T_{gel} in Fig. 1(c)]. Furthermore, T_t and T_f approach
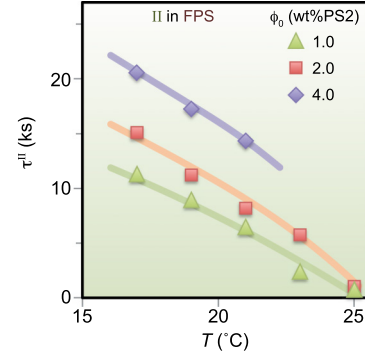

FIG. 10. Temperature dependencies of the mechanical relaxation times, τ^{II} in regime II of FPS. These values were obtained by the fitting of $\Delta\ell$ by $\Delta\ell_{fit}$ (see Appendix 4 a). Solid lines are to guide the eye.

Θ with an increase in N. Note that the Θ temperature is T_c in the limit of $N \to \infty$, where $\phi_c(N \to \infty) \to 0$ [22,33]. Similarly, T_{gel} should also approach Θ in this limit. Thus, both K_{tg} and μ_{tg} should immediately be switched on just below Θ as in a permanent gel: Phase separation of a critical polymer solution with $N \to \infty$ should basically be the same as that of a permanent gel. This provides us with a unified understanding of phase separation of polymer solutions and chemically cross linked polymer gels, which form a transient and a permanent network, respectively.
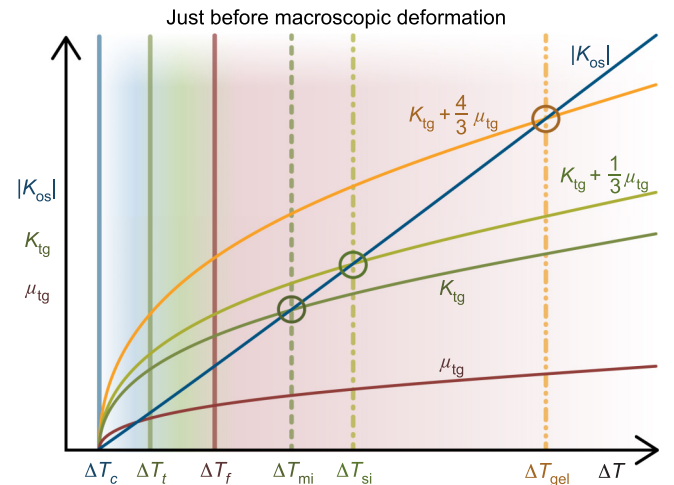

FIG. 11. Schematic figure of expected transitions as a function of the quench depth. We expect crossovers of $|K_{os}|$ with K_{tg}, $K_{tg} + \frac{1}{3}\mu_{tg}$, and $K_{tg} + \frac{4}{3}\mu_{tg}$, assuming that $K_{tg} \sim \Delta T^{\gamma'_B}$, $\mu_{tg} \sim \Delta T^{\gamma'_S}$ ($0 < \gamma'_B, \gamma'_S < 1$) and $|K_{os}| \sim \Delta T^{\gamma'}$ ($\gamma' \gtrsim 1$) [3]. These crossovers correspond to transitions of a permanent gel suggested in Refs. [29,51]: ΔT_{mi} is the macroscopic instability, ΔT_{si} is the surface instability, and ΔT_{gel} is the phase separation of a permanent gel [or GPS in Fig. 1(c)]. Even a transient gel might become unstable below ΔT_{mi} as if it were a "permanent" gel. Although only the behavior of ΔT_{gel} is explained for simplicity, we infer that the ΔT_{mi} and ΔT_{si} behave in the same manner as ΔT_{gel}.

G. Effects of boundary conditions on viscoelastic phase separation

Here we discuss the roles of boundary conditions in the pattern evolution during viscoelastic phase separation (VPS). The crucial difference between the side-cramped-disk boundary condition employed in our previous quasi-2D experiments [34,35] and the free boundary condition in the present three-dimensional experiments is that the boundary supports the self-generated mechanical stress for the former but not for the latter. For the cramped case, the fixed boundary prevents the system from shrinking as a whole, leading exclusively to the *internal* mechanical instability, or the mechanical fracture, of the transient gel [1,2,7,34,35]. This internal mechanical instability leads to characteristic patterns: creation of spherical holes for strongly viscoelastic phase separation (sVPS) [Fig. 2(b)] and creation of anisotropic cracks for fracture phase separation (FPS) [Fig. 2(c)]. On the other hand, such a stress at the boundary is absent for the free boundary condition employed in the present study. Thus, the self-generated stress directly leads to the volume shrinking of the system as a whole. Interestingly, however, the internal mechanical instability and the resulting "solvent bubble formation" can be induced even for the free boundary case (see, e.g., Fig. 8). This is similar to bubble formation formed upon shrinking of a permanent gel [27]. This should be due to slow solvent diffusion, which leads to slow volume shrinking (see above) and accordingly results in internal mechanical instability. Thus, there is a competition between macroscopic volume shrinking and shrinking via internal mechanical instability accompanied by solvent-hole creation. This balance depends on the relation between the size of a system and its viscoelastic lengths; for example, a system smaller than both ξ_S and ξ_B can shrink as a whole without internal mechanical instability. This feature may even be enhanced by the formation of a skin layer [27].

We stress that for both fixed and free boundary conditions, the basic behavior are controlled solely by the relationship between the characteristic time of deformation τ_d, the relaxation time of a transient gel for bulk deformation, τ_B, and that for shear deformation, τ_S, as indicated by relations (A)–(C). These relations (A)–(C) are then affected by the physical conditions such as the temperature T, the initial average composition ϕ_0 and the degree of polymerization of the polymer, N. Thus, there is one-to-one correspondence between wVPS, sVPS, and FPS in the fixed boundary condition and those in the free boundary condition, as discussed above.

Here it is worth pointing out an interesting similarity in the temperature dependence of their characteristic times between the two boundary conditions. When decreasing T below the onset temperature of FPS, T_f, the characteristic time of fracturing τ_c increases for the side-cramped thin film case [35], and similarly the characteristic time of shrinking also increase for the free boundary case [see the upper inset of Fig. 5(d) and also Fig. 10]. This similar tendency can be explained by the "hardening" of a transient gel due to the emergence of elasticity: For a nonclamped gel, its hardening leads to the increase in the characteristic shrinking time in regime III and regime ii (without fracture). This is because $K_{tg} + \frac{4}{3}\mu_{tg} - |K_{os}|$ [the denominator of τ^{III} in Eq. (14)] and also $K_{tg} - |K_{os}|$ [the denominator of τ^{ii} in Eq. (12)] decrease

with decreasing T: The hardening due to the increase of both K_{tg} and μ_{tg} suppresses a tendency of deformation and subdivision of the nonclamped gel represented by $|K_{os}|$ (see also Fig. 11 and Sec. V A). Thus, for a harder clamped transient gel, a stronger driving force is required for its fracture, or for creating cracks, leading to the increase in τ_c.

Finally, we mention the boundary conditions for numerical simulations. In simulations of VPS, the periodic boundary condition has so far been employed [37,54–56]. This condition corresponds to the above clamped boundary condition in experiments. It may be interesting to study VPS under fixed and free boundary conditions by numerical simulations.

VII. CONCLUSION

A transient gel state is temporally formed in the early stage of viscoelastic phase separation (VPS) of any polymer solutions. The physical understanding of this dynamical process is very challenging since transient gelation is a consequence of complex dynamical interplay between phase separation and mechanical relaxation, which takes place in a nonequilibrium process. Such an interplay may be relevant to many biological phenomena, which are basically viscoelastic multicomponent systems. Here we elucidate the physical essence of dynamical interplay in volume shrinking of a transient gel formed in polymer solutions undergoing phase separation.

We have revealed that the process of the emergence of elasticity in the early stage of phase separation is completely the reverse of its disappearance process. This is a direct consequence of the fact that both processes are controlled by viscoelastic relaxation between the competing timescales, i.e., the characteristic deformation time (τ_d) and the mechanical relaxation times (τ_B and τ_S). The emergence of elasticity is the process of the former becoming shorter than the latter, whereas its disappearance is the process of the former becoming longer than the latter. On the basis of the time relation and the switching of the relevant order parameter between the scalar and tensor ones, we also clarify the dynamics in the characteristic regimes in VPS. Furthermore, considering not only whether globules made of collapsed polymers percolate or not (the connectivity) but also how they percolate and contribute to the bulk and shear relaxation, we explain the relation of $\tau_B > \tau_S$, which is responsible not only for the emergence of three types of VPS, wVPS, sVPS, and FPS, but also for various time regimes i, ii, III, II, and I. Thus, our study has revealed the dynamically evolving nature of a transient gel state (e.g., for FPS, liquid $\rightarrow$ gel with volume elasticity $\rightarrow$ gel with volume and shear elasticity $\rightarrow$ gel with volume elasticity $\rightarrow$ condensed liquid) formed in a nonequilibrium process of phase separation.

Here we discuss a necessary condition for the emergence of a transient gel state during phase separation and the universality of transient gelation in dynamically asymmetric mixture other than polymer solutions. We argue that it is the presence of large size asymmetry between the components and the presence of a liquid component, both of which are necessary for strongly asymmetric stress division. We note that a liquid just flows without supporting any mechanical stress if the deformation induced by phase separation is slow enough. Thus, our finding should directly be applied to any

dynamically asymmetric mixtures satisfying these conditions, which include polymer solutions, colloidal suspensions, emulsions, and biological solutions such as protein solutions.

Strong dynamic asymmetry between the components can also be caused by a large difference in the glass-transition temperature of the two components [57]. This allows the characteristic deformation rate to exceed the mechanical relaxation rate. Thus, VPS itself should also be observed for mixtures of any amorphous materials such as metallic and oxide glasses. In such a case, however, we cannot expect the formation of a transient gel since there is little size asymmetry between the components of a mixture.

Finally we mention applications of transient gelation in materials science to form network (or porous) structures of a wide range of pore size. Our findings shed new light not only on the nature of a transient gel state, which is a fundamental out-of-equilibrium state of matter with network morphology, but also on its applications to materials science [4,5], food science [6,7], bioscience [8,9,21], medical science [10], and geoscience [11,12]. Porous materials of nanometer scale can be obtained by freezing a transient gel structure in the early stage, whereas those of micron-to-millimeter scale by freezing sVPS in the late stage. Nanoporous structures obtained in this way should be quite uniform since they are formed by early stage viscoelastic spinodal decomposition and thus are quite useful for applications to batteries, catalysts, and filters. On the other hand, mesoscopic porous structures can be used in structural materials with high mechanical strength and low weight, such as artificial bones, membrane filters, scaffolds for biological cells, and food science. Our study shows the importance of the boundary condition imposed on a transient gel, reflecting its mechanical nature. This boundary condition is a crucial factor for controlling the formation of porous materials. The fundamental understanding of dynamical evolution of a transient gel also provides a proper condition to form a desired porous network structure during demixing and a proper timing of structure freezing.

APPENDIX: EXPERIMENTAL AND ANALYSIS METHODS

1. Sample preparation

Here we note that the DEM solvent tends to absorb moisture, which shifts T_c upwards. To avoid this impurity effect, we dried DEM by using molecular sieves and mixed it with PS in a glove bag filled with dried N_2 gas and silica gel. Then we carefully sealed the mixture in a cylindrical glass tube, which was kept in a good solvent condition at $40\,°C$ for several days to ensure perfect mixing.

The solutions have no sol-gel transition, or do not form physical gels. The two components have a slight difference in the density (PS density is $1.04 - 1.065$ g/cm^3, DEM density is 1.055 g/cm^3), and thus the PS-rich phase always sediments

and goes to the bottom of a sample vial after phase separation. However, we minimize this gravitational effect by placing a thin cylindrical glass tube so that its long axis lies along a horizontal direction (see below).

2. Microscopy observation of phase-separation patterns and their transition temperatures

For quasi-2D experiments, we prepared a sample cell on a hot plate controlled at $40\,°C$, at which a sample is in the stable one-phase region, inside the above-described dried glove bag. We constructed the cell by sandwiching a sample solution by two cover glasses, whose gap spacing was precisely controlled by inserting a small amount of monodisperse glass beads (the diameter was either 5 or 10 μm). Then we quenched the temperature of the sample by manually transferring the cell from on a hot plate to on a temperature-controlling hot stage (Linkam TH-600), which was set for phase-contrast microscopy observation. This enables us to make a very quick temperature quench. This method was used for observations of viscoelastic phase separation (VPS) shown in Figs. 2(a)–2(c). We note that the weakly viscoelastic phase separation (wVPS) pattern shown in Fig. 2(a) is affected by wetting-layer formation of the solvent-rich phase on the glass walls [58]. Accordingly, the pattern is not a bicontinuous one expected for a symmetric composition, for which the two coexisting phases occupy the same volume [1–3], despite the nearly symmetric composition.

We measured the onset temperature of fracture phase separation (FPS), T_f [35], near ϕ_c [Fig. 1(c)] for PS of $M_w = 1.09 \times 10^6$ ($\phi_c = 4.11$ wt% PS, $T_c = 23.5\,°C$), for PS of $M_w = 8.49 \times 10^6$ ($\phi_c = 1.2$ wt% PS, $T_c = 29.2\,°C$), and for PS2, with an accuracy of ± 2 K. We note that the values of the binodal temperature T_b (including T_c), the onset temperature of strongly viscoelastic phase separation (sVPS), T_t, and T_f were reported in Refs. [34,35].

3. Preparation of sample cylinder tubes

We used, as a sample cell, a cylindrical glass tube, whose inner diameter was 1 mm and length ~ 10 cm. The amount of a sample solution was ~ 6 μl, and thus the length of a solution after injected into the cylindrical cell was nearly 8 mm. The glass tubes were flame sealed after injecting a solution, and we dipped them into a temperature-controlled water bath for observation. We carried out this flame sealing in a glove box, which was filled by dried air supplied from a chamber of silica gel connected to an air pump. This is because we need to maintain a dried condition for hygroscopic DEM as well as to supply oxygen for the flame sealing. Despite these efforts, complete avoidance of moisture was difficult because drying by silica gel is not perfect and the flame sealing inevitably generates moisture, both of which occasionally cause a slight increase in T_c.

Thus, we carefully estimated the amount of the moisture-induced shift of T_b for each sample before using it for volume-shrinking experiments. We measured T_b by gradually decreasing T of a sample and detecting T_b as the onset temperature of turbidity. Immediately after this measurement, we increased T to $40\,°C$ and kept the sample there for some days to accomplish its perfect mixing.
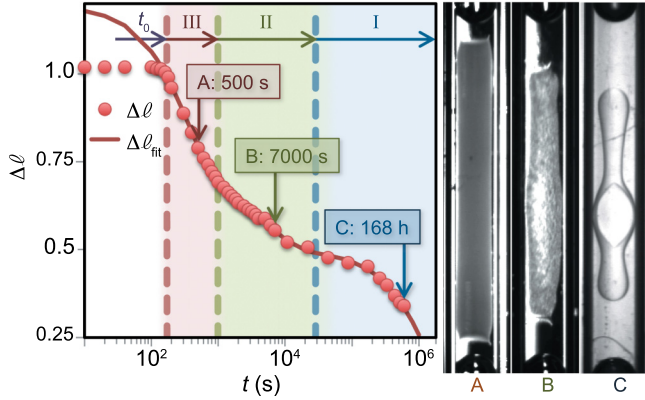
FIG. 12. Three regimes of the temporal change in the scaled gel length for a deep quench, where FPS takes place. The $\Delta\ell$ was measured from images observed for 2 wt% PS2 at 23 °C (see also images A–C observed in each regime). The solid curve is the best fit of the function $\Delta\ell_{\text{fit}}$ of triple exponentials to the data with the following fitting parameters: $\ell_0 = 7.6$ mm, $\ell_f = 3.5$ mm, $t_0 = 162$ s, $\tau^{\text{III}} = 342$ s, $\tau^{\text{II}} = 5{,}770$ s, $\tau^{\text{I}} = 1.52 \times 10^6$ s, $A^{\text{III}} = 0.310$, $A^{\text{II}} = 0.192$, and $A^{\text{I}} = 0.498$, respectively. The direction of incident light is the same for A and B, but different for C.

4. Observation of a free shrinking process of a transient gel and its characterization

A cylindrical tube containing a polymer solution was set on a sample holder horizontally to minimize the effect of gravity. The temperature quench was accomplished by quickly transferring a sample tube from on a hot plate (40 °C) to in a water bath set at a target temperature [Figs. 1(a) and 1(b)]. A process of phase separation and transient gel formation was observed with optical microscopy equipped with a CCD camera (see Videos 1–3 in the Supplemental Materials [39]), whose optical axis (normal to the image plane) was set along the direction of gravity. Digital images captured with logarithmic timing ranged from 5 s to a few days were stored in a computer. Then, the length ℓ and width (or diameter) w of a transient gel undergoing volume shrinking were measured by using the digitized image. The spatial resolutions were 12.5 μm/pixel and 20 μm/pixel for PS1-DEM and PS2-DEM, respectively. A typical example of the shrinking process of a transient gel in FPS is shown in Fig. 12.

a. Analysis of the volume-shrinking kinetics of a transient gel

The initial stage before t_0, the onset time when the large volume deformation starts, is divided into two, regimes i and ii, for sVPS and FPS (see below). We determined the terminal time of regime i, t_f^{i} (note that $t_f^{\text{i}} = t_0$ for wVPS) from the onset of the isotropic shrinking characteristic of regime ii, which induces the same decrease in $w - w_0$ and $\ell - \ell_0$, where w_0 and ℓ_0 are the initial width and length, respectively. We include regime ii to the process before t_0 although this regime involves macroscopic shrinking (the maximum amount of the shrinking width is $\sim$0.05 mm). This is because the duration of regime ii ($\sim$100 s) is much shorter than the characteristic decay time of the shrinking $\tau^{\text{ii}} \sim 10^4$ s; and thus we cannot make exponential fitting for this regime.
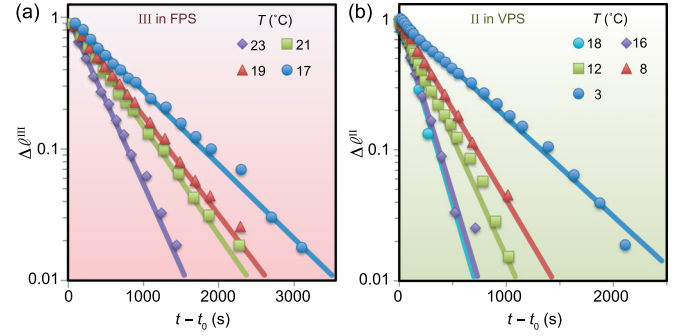

FIG. 13. Reconstructed reduced length in regime III and II. Each solid line denotes a single exponential decay. (a) $\Delta\ell^{\text{III}}(t)$ at several temperatures T for 2 wt% PS2. (b) $\Delta\ell^{\text{II}}(t)$ at several temperatures T for 4 wt% PS1.

For characterizing macroscopic deformation after t_0, we introduce the following scaled length $\Delta\ell(t)$ of a transient gel:

$$\Delta\ell(t) = \frac{\ell(t) - \ell_f}{\ell_0 - \ell_f},$$

where ℓ_f is the final length. We define similar quantities for w using the same definitions. We analyzed the temporal change of $\Delta\ell(t)$ by fitting the following function:

$$\Delta\ell_{\text{fit}}(t) = \sum_k A^k \exp\left(-\frac{t - t_0}{\tau^k}\right),$$

where $k = \text{I}, \text{II},$ or III, A^k is a constant satisfying $\sum_k A^k = 1$, t_0 is the induction time, τ^k is the relaxation time of regime k with $\tau^{\text{III}} < \tau^{\text{II}} < \tau^{\text{I}}$. This functional form is reasonable when the regimes are rather well separated, which is actually the case as can be seen in Fig. 12 (see also its legend). We note that the number of regimes in the deformation process depends on each phase separation type: wVPS has $k = \text{I}$ only; sVPS has $k = \text{I}$ or II (Fig. 4); FPS has $k = \text{I}, \text{II}$ or III (see Fig. 12).

We calculated the scaled gel length in regime III, $\Delta\ell^{\text{III}}$, and that in regime II, $\Delta\ell^{\text{II}}$ as follows:

$$\Delta\ell^{\text{III}}(t) = \frac{\ell(t) - A^{\text{I}}\exp\left(-\frac{t-t_0}{\tau^{\text{I}}}\right) - A^{\text{II}}\exp\left(-\frac{t-t_0}{\tau^{\text{II}}}\right)}{A^{\text{III}}},$$

$$\Delta\ell^{\text{II}}(t) = \frac{\ell(t) - A^{\text{I}}\exp\left(-\frac{t-t_0}{\tau^{\text{I}}}\right)}{A^{\text{II}}}.$$

We estimated the ending times of regimes III and II, which we refer to t_{lf}^{III} and t_{lf}^{II}, respectively, as the times when $\Delta\ell^{\text{III}}(t)$ and $\Delta\ell^{\text{II}}(t)$ reached 0.05, respectively. We show examples of such analysis in Fig. 13.

We also calculated the strain $-\gamma_\ell = (\ell - \ell_0)/\ell_0$ and its final value in regime III, $-\gamma_\ell^{\text{III}}$, by using the final length in regime III, ℓ_f^{III}, estimated from $A^{\text{III}} = (\ell_0 - \ell_f^{\text{III}})/(\ell_0 - \ell_f)$ (Fig. 6). Similarly, the final strain value in regime II, $-\gamma_\ell^{\text{II}}$, was obtained from ℓ_f^{II} estimated from $A^{\text{II}} = (\ell_f^{\text{III}} - \ell_f^{\text{II}})/(\ell_0 - \ell_f)$.

b. Characterization of the inner structure of transient gels

The distribution of the light intensity $I(t)$ transmitted through a transient gel was measured with a resolution of 256 to characterize its internal structure. Note that a sample cell
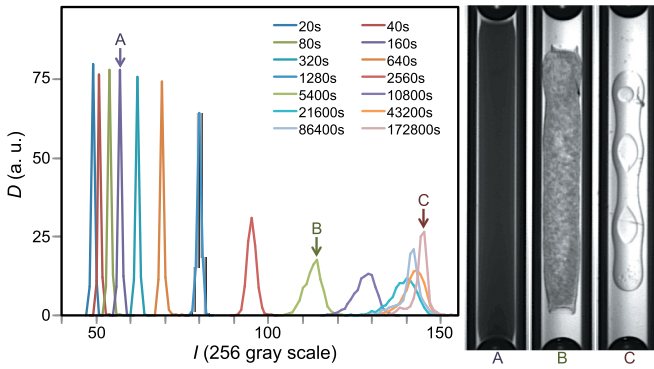
FIG. 14. Temporal change of the transmitted light intensity through a transient gel. The transmitted light intensity I and its distribution $D(I)$ were measured from images observed for 2 wt% PS2 at 25 °C, including A (160 s), B (1.5 h), and C (48 h).

was illuminated from its back. The average of $I(t)$, $\langle I(t) \rangle$, and the variance of the intensity fluctuations, $(\langle \Delta I^2(t) \rangle)^{1/2}$, were calculated from the distribution function of $I(t)$, $D(I(t))$ (Fig. 14), by using image analysis software (Digimo Imagehyper 2). A part of a transient gel with a rectangular shape was used for this analysis by excluding its boundary parts with the width of 5–10 pixels. $D(I(t))$ estimated in this way has almost the Gaussian distribution (Fig. 14). Then we calculated $\langle I(t) \rangle$ and $(\langle \Delta I^2(t) \rangle)^{1/2}$ as follows:

$$\langle I(t) \rangle = C_I \frac{\sum_{I=0}^{255} I(t) D(I(t))}{\sum_{I=0}^{255} D(I(t))},$$

$$\sqrt{\langle \Delta I^2(t) \rangle} = C_v \sqrt{\frac{\sum_{I=0}^{255} I^2(t) D(I(t))}{\sum_{I=0}^{255} D(I(t))} - \langle I(t) \rangle^2},$$

where C_I and C_v are positive constants.

Here we summarize the temporal change in the intensity distribution, which reflects the change in the internal structure of a transient gel. There are basically three time regimes: just after the initiation of phase separation, the entire sample solution becomes dark due to strong multiple scattering of the incident light by spatial fluctuations of the composition, whose correlation length is comparable to the wavelength of the light. This leads to the sharpening of $D(I)$ [i.e., the decrease in $(\langle \Delta I^2 \rangle)^{1/2}$] and the decrease in $\langle I \rangle$ (Fig. 14 A). Then, the transient gel becomes brighter and its internal structure becomes visible since the characteristic size of the structure starts to exceed the wavelength of the light, resulting in the decrease in the scattering. This leads to the broadening of $D(I)$ [i.e., the increase in $(\langle \Delta I^2 \rangle)^{1/2}$] and the increase in $\langle I \rangle$ (Fig. 14 B). Finally, the transient gel becomes transparent since the DEM-rich domains trapped in a transient gel gradually escape from the matrix phase and merges to the surrounding DEM-rich phase. This leads to the sharpening of $D(I)$ again [i.e., the decrease in $(\langle \Delta I^2 \rangle)^{1/2}$] and results in the large value of $\langle I \rangle$ (Fig. 14 C). We note that $(\langle \Delta I^2 \rangle)^{1/2}$ in the last regime is broaden by shadows of the interfaces of large DEM-rich droplets. Since this is a kind of artifact due to droplet interfaces and the geometry of a cylindrical tube, we remove the contribution from interface shadows in the plot of $(\langle \Delta I^2 \rangle)^{1/2}$ shown in Figs. 3–5 (see Sec. III).

[1] H. Tanaka, Viscoelastic phase separation, J. Phys.: Condens. Matter **12**, R207 (2000).

[2] H. Tanaka, *Soft interfaces: Lecture Notes of the Les Houches Summer School* (Oxford University Press, Oxford, 2017), Chap. 13.

[3] A. Onuki, *Phase Transition Dynamics* (Cambridge University Press, Cambridge, 2002).

[4] G. Yu, J. Gao, J. C. Hummelen, F. Wudl, and A. J. Heeger, Polymer photovoltaic cells: Enhanced efficiencies via a network of internal donor-acceptor heterojunctions, Science **270**, 1789 (1995).

[5] K. Nakanishi, Pore structure control of silica gels based on phase separation, J. Porous Mater. **4**, 67 (1997).

[6] R. Mezzenga, P. Schurtenberger, A. Burbidge, and M. Michel, Understanding foods as soft materials, Nat. Mater. **4**, 729 (2005).

[7] H. Tanaka, Viscoelastic phase separation in soft matter and foods, Faraday Discuss. **158**, 371 (2012).

[8] E. R. Dufresne, H. Noh, V. Saranathan, S. G. J. Mochrie, H. Cao, and R. O. Prum, Self-assembly of amorphous biophotonic nanostructures by phase separation, Soft Matter **5**, 1792 (2009).

[9] K. Richter, M. Nessling, and P. Lichter, Macromolecular crowding and its potential impact on nuclear function, BBA-Mol. Cell Res. **1783**, 2100 (2008).

[10] Y. S. Nam and T. G. Park, Porous biodegradable polymeric scaffolds prepared by thermally induced phase separation, J. Biomed. Mater. Res. **47**, 8 (1999).

[11] A. H. Shen and H. Keppler, Direct observation miscibility in the albite-H$_2$O system, Nature (London) **385**, 710 (1997).

[12] J.-L. Vigneresse and J. P. Burg, Strain-rate-dependent rheology of partially molten rocks, Geol. Soc. London Spec. Publ. **227**, 327 (2004).

[13] D. M. Mitrea and R. W. Kriwacki, Phase separation in biology; functional organization of a higher order, Cell Commun. Signaling **14**, 1 (2016).

[14] M. Feric, N. Vaidya, T. S. Harmon, D. M. Mitrea, L. Zhu, T. M. Richardson, R. W. Kriwacki, R. V. Pappu, and C. P. Brangwynne, Coexisting liquid phases underlie nucleolar subcompartments, Cell (Cambridge, MA, U.S.) **165**, 1686 (2016).

[15] L.-P. Bergeron-Sandoval, N. Safaee, and S. W. Michnick, Mechanisms and consequences of macromolecular phase separation, Cell (Cambridge, MA, U.S.) **165**, 1067 (2016).

[16] A. Aguzzi and M. Altmeyer, Phase separation: Linking cellular compartmentalization to disease, Trends Cell Biol. **26**, 547 (2016).

[17] A. R. Strom, A. V. Emelyanov, M. Mir, D. V. Fyodorov, X. Darzacq, and G. H. Karpen, Phase separation drives heterochromatin domain formation, Nature (London) **547**, 241 (2017).

[18] A. G. Larson, D. Elnatan, M. M. Keenen, M. J. Trnka, J. B. Johnston, A. L. Burlingame, D. A. Agard, Sy Redding, and G. J. Narlikar, Liquid droplet formation by hp1α suggests a role for phase separation in heterochromatin, Nature (London) **547**, 236 (2017).

[19] Y. Shin and C. P. Brangwynne, Liquid phase condensation in cell physiology and disease, Science **357**, eaaf4382 (2017).

[20] S. F. Banani, H. O. Lee, A. A. Hyman, and M. K. Rosen, Biomolecular condensates: Organizers of cellular biochemistry, Nat. Rev. Mol. Cell Biol. **18**, 285 (2017).

[21] F. J. Iborra, Can visco-elastic phase separation, macromolecular crowding and colloidal physics explain nuclear organisation? Theor. Biol. Med. Modell. **4**, 15 (2007).

[22] M. Doi and S. F. Edwards, *The Theory of Polymer Dynamics* (Clarendon Press, Oxford, 1986).

[23] R. G. Larson, *The Structure and Rheology of Complex Fluids* (Oxford University Press, New York, 1999), Vol 33.

[24] T. Tanaka, L. O. Hocker, and G. B. Benedek, Spectrum of light scattered from a viscoelastic gel, J. Chem. Phys. **59**, 5151 (1973).

[25] T. Tanaka and D. Fillmore, Kinetics of swelling of gels, J. Chem. Phys. **70**, 1214 (1979).

[26] T. Tanaka, S.-T. Sun, Y. Hirokawa, S. Katayama, J. Kucera, Y. Hirose, and T. Amiya, Mechanical instability of gels at the phase transition, Nature (London) **325**, 796 (1987).

[27] E. S. Matsuo and T. Tanaka, Kinetics of discontinuous volume-phase transition of gels, J. Chem. Phys. **89**, 1695 (1988).

[28] Y. Li and T. Tanaka, Kinetics of swelling and shrinking of gels, J. Chem. Phys. **92**, 1365 (1990).

[29] A. Onuki, Theory of Phase Transition in Polymer Gels, in *Advances in Polymer Science*, edited by K. Dušek (Springer-Verlag, Berlin, 1993), Vol. 109, p. 63.

[30] C. Wang, Y. Li, and Z. Hu, Swelling kinetics of polymer gels, Macromolecules (Washington, DC, U.S.) **30**, 4727 (1997).

[31] T. Yamaue and M. Doi, The stress diffusion coupling in the swelling dynamics of cylindrical gels, J. Chem. Phys. **122**, 084703 (2005).

[32] M. Doi, Gel dynamics, J. Phys. Soc. Jpn. **78**, 052001 (2009).

[33] P. G. de Gennes, *Scaling Concepts in Polymer Physics* (Cornell University Press, New York, 1979).

[34] T. Koyama and H. Tanaka, Generic kinetic pathway of phase separation of deeply quenched polymer solutions: Transient gelation, Europhys. Lett. **80**, 68002 (2007).

[35] T. Koyama, T. Araki, and H. Tanaka, Fracture Phase Separation, Phys. Rev. Lett. **102**, 065701 (2009).

[36] A. Furukawa and H. Tanaka, Inhomogeneous flow and fracture of glassy materials, Nat. Mater. **8**, 601 (2009).

[37] H. Tanaka and T. Araki, Phase Inversion During Viscoelastic Phase Separation: Roles of Bulk and Shear Relaxation Moduli, Phys. Rev. Lett. **78**, 4966 (1997).

[38] A. Furukawa and H. Tanaka, Violation of the incompressibility of liquid by simple shear flow, Nature (London) **443**, 434 (2006).

[39] See Supplemental Material at http://link.aps.org/supplemental/10.1103/PhysRevE.98.062617 for phase-separation processes in PS-DEM in cylinders with 1-mm diameter. Video 1 shows wVPS and sVPS for 8 and 4 wt% PS1, respectively, at 16°C in PS1-DEM. Video 2 shows sVPS for both 4 and 8 wt% PS1 at 12°C in PS1-DEM. Video 3 shows FPS for all 1, 2 and 4 wt% PS2 at 19°C in PS2-DEM.

[40] H. Tanaka and T. Araki, Spontaneous coarsening of a colloidal network driven by self-generated mechanical stress, Europhys. Lett. **79**, 58003 (2007).

[41] A. Furukawa and H. Tanaka, Key Role of Hydrodynamic Interactions in Colloidal Gelation, Phys. Rev. Lett. **104**, 245702 (2010).

[42] H. Verduin and J. K. G. Dhont, Phase diagram of a model adhesive hard-sphere dispersion, J. Colloid Interface Sci. **172**, 425 (1995).

[43] N. A. M. Verhaegh, J. S. van Duijneveldt, J. K. G. Dhont, and H. N. W. Lekkerkerker, Fluid-fluid phase separation in colloid-polymer mixtures studied with small angle light scattering and light microscopy, Phys. A (Amsterdam, Neth.) **230**, 409 (1996).

[44] W. C. K. Poon, L. Starrs, S. P. Meeker, A. Mousaid, R. M. L. Evans, P. N. Pusey, and M. M. Robins, Delayed sedimentation of transient gels in colloid-polymer mixtures: Dark-field observation, rheology and dynamic light scattering studies, Faraday Discuss. **112**, 143 (1999).

[45] V. J. Anderson and H. N. W. Lekkerkerker, Insights into phase transition kinetics from colloid science, Nature (London) **416**, 811 (2002).

[46] A. Shalkevich, A. Stradner, S. K. Bhat, F. Muller, and P. Schurtenberger, Cluster, glass, and gel formation and viscoelastic phase separation in aqueous clay suspensions, Langmuir **23**, 3570 (2007).

[47] P. J. Lu, E. Zaccarelli, F. Ciulla, A. B. Schofield, F. Sciortino, and D. A. Weitz, Gelation of particles with short-range attraction, Nature (London) **453**, 499 (2008).

[48] V. Testard, L. Berthier, and W. Kob, Intermittent dynamics and logarithmic domain growth during the spinodal decomposition of a glass-forming liquid, J. Chem. Phys. **140**, 164502 (2014).

[49] J. Colombo and E. Del Gado, Self-assembly and cooperative dynamics of a model colloidal gel network, Soft Matter **10**, 4003 (2014).

[50] M. Doi and A. Onuki, Dynamic coupling between stress and composition in polymer solutions and blends, J. Phys. II (Paris) **2**, 1631 (1992).

[51] A. Onuki and T. Taniguchi, Viscoelastic effects in early stage phase separation in polymeric systems, J. Chem. Phys. **106**, 5761 (1997).

[52] P. Štěpánek and Č. Koňák, Quasielastic light scattering from polymers, colloids and gels, Adv. Colloid Interface Sci. **21**, 195 (1984).

[53] N. Toyoda, M. Takenaka, S. Saito, and T. Hashimoto, Experimental studies of stress-diffusion coupling in semi-dilute polymer solutions. I. 'Viscoelastic length' and viscoelastic effects on early stage spinodal decomposition, Polymer **42**, 9193 (2001).

[54] T. Taniguchi and A. Onuki, Network Domain Structure in Viscoelastic Phase Separation, Phys. Rev. Lett. **77**, 4910 (1996).

[55] T. Araki and H. Tanaka, Three-dimensional numerical simulation of viscoelastic phase separation: Morphological characteristics, Macromolecules (Washington, DC, U.S.) **34**, 1953 (2001).

[56] T. Araki and H. Tanaka, Simple tools for complex phenomena: Viscoelastic phase separation captured by disconnectable springs, Phys. Rev. E **72**, 041509 (2005).

[57] H. Tanaka, Universality of Viscoelastic Phase Separation in Dynamically Asymmetric Fluid Mixtures, Phys. Rev. Lett. **76**, 787 (1996).

[58] H. Tanaka, Interplay between wetting and phase separation in binary fluid mixtures: Roles of hydrodynamics, J. Phys.: Condens. Matter **13**, 4637 (2001).